Enhanced long-acting simvastatin delivery *via* effervescent powder-carrying hollow microneedles and nanocrystal-loaded microneedles

Nuoya Qin, Mingshan Li, Lalitkumar K. Vora, Ke Peng, Akmal Hidayat Bin Sabri, Yushi Tao, Alejandro J. Paredes, Helen O. McCarthy, Ryan F. Donnelly [*]

School of Pharmacy, Queen's University Belfast, Medical Biology Centre, 97 Lisburn Road, Belfast BT9 7BL, UK

ARTICLE INFO

ABSTRACT

Hyperlipidemia and its associated cardiovascular complications are the major causes of mortality and disability worldwide. Simvastatin (SIM) is one of the most commonly prescribed lipid-lowering drugs for the treatment of hyperlipidemia by competitive inhibition of 3-hydroxy-3-methylglutaryl coenzyme A (HMG-CoA) reductase. However, the extensive first-pass metabolism leading to low oral bioavailability and frequent daily doses may lead to poor patient compliance and adverse effects caused by plasma fluctuations. To overcome these challenges, this work purposed two microneedle (MN) delivery strategies for the potential enhancement of SIM delivery. Firstly, nanocrystal (NC) formulations of SIM were investigated, followed by incorporation into a tri-layer dissolving microneedle (DMN) design. Furthermore, a novel effervescent powder-carrying MN (EMN) design was developed to enhance intradermal delivery by incorporating the effervescent agents into the drug powder. Both MN approaches exhibited significantly improved permeation and in-skin deposition ability in the Franz cell study, with the *ex vivo* delivery efficiency of 64.33 ± 6.17 % and 40.11 ± 4.53 % for EMNs and DMNs, respectively. Most importantly, *in vivo* studies using a female *Sprague-Dawley* rat model confirmed the successful delivery of SIM from NCs-loaded DMNs ($C_{max} = 287.39 \pm 106.82$ ng/mL) and EMNs ($C_{max} = 203.05 \pm 17.07$ ng/mL) and maintain therapeutically relevant plasma concentrations for 15 days following a single application. The enhanced bioavailabilities of DMNs and EMNs were 24.28 % and 103.82 %, respectively, which were both significantly higher than that of conventional oral administration.

1. Introduction

Hyperlipidemia is a common medical condition affecting millions of people worldwide (Owens et al., 2014) and is characterised by elevated low-density lipoprotein (LDL), total cholesterol and triglyceride levels and reduced high-density lipoprotein (HDL) levels (Shattat, 2014). Elevated plasma lipid levels are among the prevalent risk factors associated with cardiovascular disease (CVD) (Liu et al., 2022), which is regarded as the leading cause of death and disability globally.

Simvastatin (SIM), one of the most commonly prescribed statins in commercially available pharmaceutical formulations for the treatment of hyperlipidemia, can significantly reduce the total cholesterol and LDL levels and induce a modest increase in plasma HDL levels *via* a competitive inhibition of HMG-CoA reductase (Belay et al., 2007; Eiland and Luttrell, 2010). SIM is a prodrug that is administered in the inactive lactone form, absorbed in the intestine and converted into the active β-hydroxy acid (SIMA) metabolite by CYP3A4 in the liver. Presently, the commercially available form of SIM is ingested orally, including *via* tablets and oral suspensions, with doses of 5, 10, 20, 40 and 80 mg per day. At the highest dose of 80 mg, a mean reduction in the LDL level can be achieved by 48 %. Unfortunately, SIM undergoes extensive first-pass metabolism in the intestinal gut and liver and is poorly absorbed across the gastrointestinal (GI) tract due to its extremely low water solubility (Zhang et al., 2013). Therefore, the oral bioavailability of SIM is less than 5 % (Shitara and Sugiyama, 2006). Additionally, frequent daily dosing may affect the life quality of patients and reduce compliance with medications (Parker et al., 2013; Shattat, 2014). As a result, the development of an efficient long-acting delivery system to evade first-pass

---

metabolism and improve solubility issues is necessary.

Microneedles (MNs) are minimally invasive devices that can bypass the *stratum corneum (SC)* barrier, thereby allowing drug molecules to enter the microcirculation and achieve systemic delivery *via* intradermal routes (Larrañeta et al., 2016). Conventional MN preparations often encounter challenges related to the water solubility of drugs. SIM is an extremely hydrophobic compound with a water solubility of 6.3 µg/mL and a Log P of 4.4 (Zhang et al., 2013). This work, therefore, developed two MN delivery strategies to improve bioavailability and simplify the preparation process. First, SIM was formulated into nanocrystals (NCs) using wet media milling techniques and then, loaded into the rapidly separable trilayer dissolving MNs (DMNs). NCs are nanoparticles made of the pure drug with crystalline properties, stabilised by a thin layer of surfactant or polymer (Müller et al., 2011). Because of their large specific surface, NCs lead to an enhanced drug dissolution rate and have been used to deliver drugs via multiple administration routes (McGuckin et al., 2022). The uniform particle size distribution of the NCs enables the drug-encapsulated formulation to be homogeneously distributed at the needle tips. Upon skin insertion, the intermediate layer rapidly dissolves in the presence of interstitial fluid and deposits the needle tips beneath the skin. The water-soluble backbone matrix dissolves over time, and the NCs are subsequently released into deeper viable tissues (Vora et al., 2018). The development included a comprehensive screening of the nanoformulations as well as characterisation of the NCs loaded DMN. The other strategy is a novel effervescent powder-carrying hollow microneedle (EMN) system, which is an innovation of previous pure powder-carrying MN (PMN) strategies (He et al., 2024). To date, PMNs investigation for directly dry powder delivery included insulin (Kim et al., 2020), Bacille Calmette–Guerin (BCG) vaccines (Chen et al., 2017) and tofacitinib citrate (Cárcamo-Martínez et al., 2021), where most of them possessed high water solubility. In this work, SIM as an extremely hydrophobic drug was applied in this system, utilising effervescent agents as excipients. After application, the polymeric shell dissolve in a short time when contact with the interstitial fluid and the powder loaded inside is then deposited for release (Kim et al., 2020). Instead of loading pure drug powder, in this work, effervescent agents were introduced for the first time into the powder formulations. This design is proposed to disperse the drug powder more uniformly in the skin by the bubble generation, leading to higher contact area of drug particles with the interstitial fluid, which can potentially enhance the permeability. Moreover, the effervescence may weaken the connection of the drug-laden tips with the 3D-printed baseplate, thereby enhancing the in-skin deposition performance for the sustained release purpose. Such a drug powder filling approach can potentially simplify the MN fabrication problems caused by hydrophobic compounds and water-soluble backbone matrices. In addition, keeping the drug in a dry state may correspondingly reduce the possibility of chemical reactions, and any stability issues and activity loss during the fabrication process, therefore, can be circumvented in this way (Cárcamo-Martínez et al., 2021).

This work proposed, for the first time, the concept of enhancing the intradermal delivery of the hydrophobic compound SIM dry powder with the assistance of an effervescent agent. These included a comprehensive screening of the polymeric hollow shell and MN characterisation. Both DMNs and EMNs were subjected to *ex vivo* studies to evaluate drug permeation and deposition performance by comparison with their control group (crude SIM-loaded DMNs and pure SIM-loaded PMNs), and *in vivo* delivery performance was assessed in subsequent animal studies.

2. Materials

Simvastatin was purchased from Enke Pharma-tech (Cangzhou, China). Simvastatin hydroxy acid was purchased from Biosynth® Carbosynth (Compton, UK). Acetonitrile (for HPLC, gradient grade, ≥ 99.9 %) was purchased from Sigma-Aldrich (Poole, Dorset, UK). Poly(vinyl

pyrrolidone) (PVP) (MW 58 kDa, marketed as Plasdone™ k29/32) was purchased from Ashland (Kidderminster, UK). Phosphoric acid (85 %) and formic acid were purchased from Fluorochem (Derbyshire, UK). Poloxamers 188 and 407 were purchased from BASF (Geismar, LA, USA). Hydroxyethyl cellulose (HEC) (MW 250 kDa), citric acid monohydrate, sodium bicarbonate, phosphate buffered saline (PBS) (pH 7.4), carboxymethylcellulose (CMC), poly(vinyl alcohol) (PVA) (80 % hydrolysed, MW 9–10 kDa and MW 31–50 kDa) and sodium dodecyl sulfate (SDS) were purchased from Sigma-Aldrich (St. Louis, MO, USA). The full-thickness porcine skins were collected from the stillborn piglets within 24 h postmortem and stored in a freezer (−20 °C) until further usage. Female *Sprague-Dawley* rats were purchased from Charles River Laboratories (Harlow, UK).

3. Methods

3.1. Effervescent hollow MNs

3.1.1. Fabrication of dissolvable hollow shells

Hollow dissolvable shells were fabricated by micromoulding technology. Briefly, polydimethylsiloxane (PDMS) moulds consisting of 25 conical needles (5×5 array arranged on a 0.25 cm^2 area, 1.1 mm needle height and 70 µm interspacing) were utilised for manufacturing. Dissolvable and degradable polymers with different molecular weights and concentrations were tested and are summarised in Table 1. The hollow shells were prepared by pouring 60 µL of polymer aqueous solution onto the moulds followed by centrifugation for 10 min at 3500 rpm at ambient temperature. During the process of dissection, the polymer filling the needle holes of the moulds gradually formed grooves as the water evaporated and finally generated a solidified shell structure. A round baseplate with a diameter of 8 mm and a thickness of 0.6 mm was 3D-printed from poly(lactic acid) (PLA) (Ultimaker, Geldermalsen, Netherlands) material and adhered to the solidified hollow shell using 60 % w/w PVP (58 kDa) ethanol solution as a glue. The solidified needle shells were carefully demoulded to avoid damage.

3.1.2. Rationalisation of dissolvable hollow shells

Shells of EMNs fabricated from the above 8 formulations (SF1-SF8) were screened primarily by observing their morphological appearance and comparing the loading capacity of the hollow space, dissolution rate and mechanical properties of the hollow structure. The capacities of the needle shells were compared by measuring the percentage of cavity height with a digital light microscope (Leica Microsystems, Milton Keynes, Buckinghamshire, U.K.), which was calculated using Eq. (1). The dissolution time of the polymeric shell was characterised by immersing in 10 mL of 1 % w/v SDS in PBS preheated to 37 °C. The samples were stirred individually with magnetic bars at 600 rpm at 37 °C throughout the experiment. The time required for complete dissolution was recorded as the dissolution time in seconds. The ability of the hollow shell to withstand compression was tested using a TA.XT. Plus Texture Analyser (Stable MicroSystems Ltd., Godalming, Surrey, U.K.) on eight layers of Parafilm M® with a thickness of 127 µm (Larrañeta et al., 2014). The probe was moved vertically downward at a speed of 1 mm/s with a consistent force of 32 N for 30 s. After the compression, the

Table 1
Composition of the various formulations used for the dissolvable shell.

Formulation	Composition [w/w]
SF1	40 % PVP (58 kDa)
SF2	20 % PVP (58 kDa)
SF3	30 % PVA (9–10 kDa)
SF4	20 % PVA (9–10 kDa)
SF5	20 % PVA (31–50 kDa) & 20 % PVP (58 kDa)
SF6	20 % PVA (31–50 kDa)
SF7	10 % CMC
SF8	5 % HEC

length of each needle was measured by the digital light microscope (Vora et al., 2017), and the percentage of height reduction was calculated using Eq. (2), where H_{BC} and H_{AC} represent the heights of one individual needle before and after compression, respectively.

$$\% Microcavity Height = \frac{Height of the hollow space}{Length of the needle} \quad (1)$$

$$\% Height Reduction = \frac{H_{BC} - H_{AC}}{HBC} \quad (2)$$

3.1.3. Fabrication of the SIM-loaded EMNs

The EMNs were fabricated *via* a mould-casting method, as shown in Fig. 1. After the fabrication of the polymeric shell described in section 3.1.1, the solidified needle shell was kept in the MN mould and powder formulations were loaded into the microcavities by centrifuging at 3500 rpm for 10 min. The powder formulations were designed with gradually increasing amounts of effervescent components as shown in Table 2, where EF1 (pure SIM powder) served as a control group for comparison. All powder formulations were ground manually in a mortar before loading to make them more homogenous. Afterwards, a 3D-printed PLA baseplate was then adhered to the needle shell using a 60 % w/w PVP (58 kDa) ethanol solution. The PLA filaments in the baseplate design were not dense, allowing the evaporation of the ethanol solvent in the PVP solution through it. The samples were placed on a flat surface and desiccated for 24 h at ambient temperature. Fully dried EMNs were detached from the moulds carefully and then placed in a sealed 24-well plastic plate for storage.

3.1.4. Characterisation of SIM loaded EMNs

The morphology of the EMNs was visualised by the digital light microscope. Images of the samples were obtained under various magnifications. The robustness and insertion ability of the EMNs were characterised in the similar manner to those of the polymeric shell as described in section 3.1.2. After applying a force of 32 N to eight layers of Parafilm M® for 32 s using the TA.XT (Larrañeta et al., 2014). The height reduction was reported and calculated. The percentage of holes created per layer was observed under the digital microscope and calculated using Eq. (3). The insertion depth was simulated by visualising the penetration layer of EMNs using the same protocol under a EX1301 VivoSight® optical coherence tomography (OCT) (Michelson Diagnostics Ltd, Kent, UK). Cross-sectional images of the EMNs inserted

Table 2
Powder formulations with increased amounts of effervescent agents for EMN fabrication.

|	SIM [w/w %]	Sodium Bicarbonate [w/w %]	Citric acid [w/w %]
EF1	100	0	0
EF2	50	25	25
EF3	33.3	33.3	33.3

into the Parafilm M® sheets were obtained. The predicted delivery depth of the three EMNs was compared by measuring the percentage of drug powder height in the cavity using Eq. (4). To investigate the drug content, individual EMNs were dissolved in 5 mL of deionised water and stirred on a hotplate at 600 rpm for two hours to achieve complete dissolution of the polymer matrices. Following this, an aliquot of 100 μL of suspension was diluted 10-fold by adding 900 μL of ACN. This mixture was then vortexed and centrifuged at 14,800 rpm for 10 min. The supernatant was collected and the drug content was quantified by RP-HPLC.

$$\% \, Holes \, created \, = \frac{Numbers \, of \, holes \, observed}{Numbers \, of \, needles \, per \, DMNs} \times 100\% \quad (3)$$

$$\% \, Height \, proportion \, = \frac{Height \, of \, the \, powder \, formulation}{Length \, of \, the \, needle} \quad (4)$$

3.1.5. Skin extraction and recovery of EMNs

To ensure the skin extraction method was efficient for further *ex vivo* deposition studies without any degradation in the presence of the skin, the recovery of SIM from excised full-thickness porcine skin was investigated. The skin samples were cut into small fragments and mixed with 20 mg powder formulations. Two stainless steel beads (5 mm diameter) were added to the blends, followed by disruption *via* a Tissue Lyser (Qiagen, Ltd, Manchester, UK) for 15 min at 50 Hz. Afterwards, 1 mL of acetonitrile (ACN) was used to extract the drug and the samples were homogenised for another cycle. The aqueous skin blends were diluted with ACN and sonicated for 30 min. The obtained solutions were centrifuged at 14,800 rpm for 10 min, and the supernatants were collected for further HPLC analysis. The control group was subjected to the same conditions without the involvement of skin fragments. The recovery efficiency of SIM from porcine skin was calculated using Eq. (5).
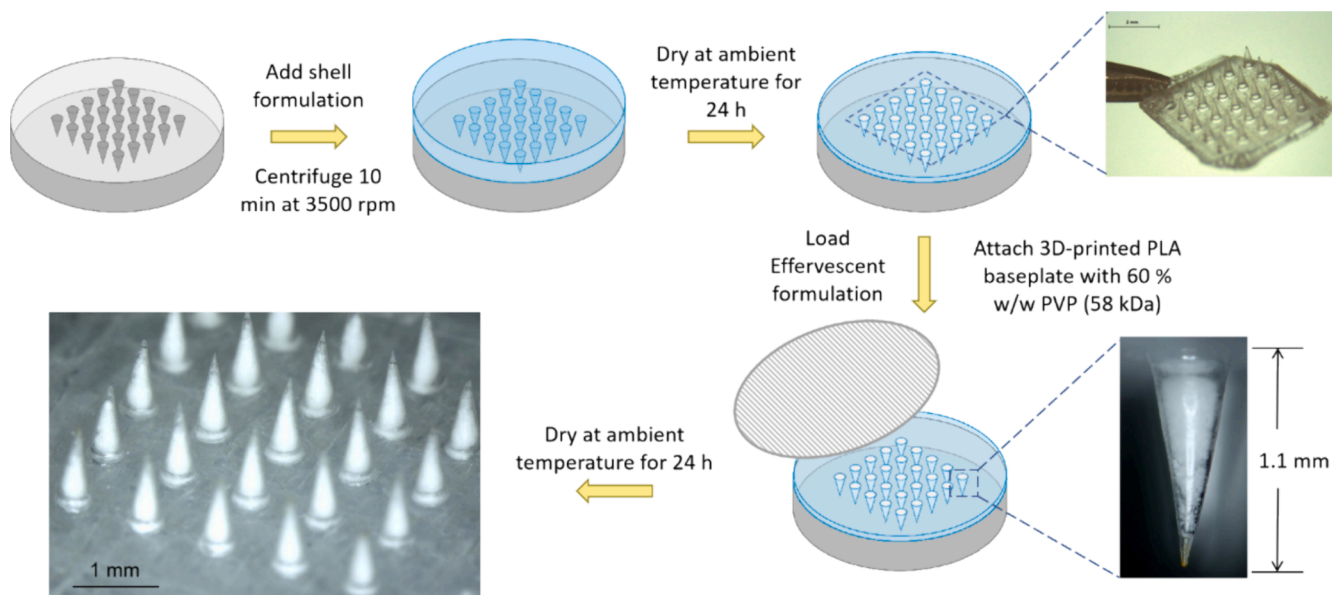
Fig. 1. Schematic representation of the fabrication process of SIM loaded EMNs.

$$\% \text{ SIM recovery in skin} = \frac{\text{Drug content in experiment group}}{\text{Drug content in control group}} \times 100\% \quad (5)$$

3.2. Dissolving MNs

3.2.1. Fabrication and rationalisation of SIM NCs

The nanosuspension (NS) was formulated *via* a top-down approach by wet bead milling at the laboratory-scale. Briefly, a sealed milling vessel containing unprocessed SIM particles, ceramic beads with a diameter of 0.1–0.2 mm, an aqueous surfactant/polymer solution as the stabiliser, and magnetic stirrers were used for milling, following previously reported protocols (Zhang et al., 2023a). To obtain the SIM NCs, the freshly prepared SIM NS was lyophilised to remove the residual solvent in the matrix for further DMN fabrication. The samples were prefrozen at −80 °C for at least 1 h and subsequently transferred to a Virtis Advantage Bench Top Freeze Drier (SP Scientific Ltd., Warminster, PA). To achieve a low particle size, the method is rationalised gradually by selecting stabilisers and monitoring the particle size changes under different milling periods (3 h, 6 h, 9 h, 24 h). Drug content was then improved based on the selected stabiliser. The details of the rationalisation parameters are presented in Table 3 and Table 4.

3.2.2. Measurement of the particle size, PDI and drug content of SIM NCs

The particle size distribution of the coarse SIM powder was detected by a Malvern Mastersizer 3000 (Malvern Panalytical Ltd., Swords, Dublin, Ireland). Briefly, 5 mg/ml of SIM dispersed in Tween 80 was added dropwise to the 500 mL beaker of the Mastersizer filled with deionised water until the required obscuration level of 3–5 % was reached, followed by agitation at 2000 rpm throughout the period. The particle size and PDI of the fabricated SIM NS were characterised *via* dynamic light scattering (DLS) (NanoBrook Omni® analyser, Brookhaven Instruments Corporation, New York, USA). An aliquot of 10 μL of NS sample was taken and transferred into a poly(styrene) cuvette cell and reconstituted with 3 mL deionised water. To evaluate the drug content of the SIM NCs, 5 mg of lyophilised NC powder was weighed and redissolved in 2 mL deionised water in a 2 mL Eppendorf® tube. Afterwards, the samples were diluted 50 times and vortexed for at least 30 s and then centrifuged at 14,000 rpm for 15 min. The supernatants were collected and the drug content was subsequently analysed *via* HPLC-UV.

3.2.3. Fabrication of SIM NCs-loaded trilayer DMNs

The trilayer DMNs were prepared *via* a micromoulding process with SIM NCs located only in the needle tips. PVA (9–10 kDa) and PVP (58 kDa) were used as the matrices for DMN fabrication. Initially, SIM NCs (200 mg) were homogenised with 120 mg of PVA-PVP aqueous solution (1:1 w/w mixture of 40 % w/w PVA 10 kDa and 40 % w/w PVP 58 kDa) and 175 mg of deionised water using the SpeedMixer at 3500 rpm for 5 min. Coarse SIM-loaded DMNs with identical theoretical drug loading (30 % w/w) were then fabricated using the same method as a control group. The aqueous blend was evenly poured onto a prefabricated silicone mould consisting of 600 pyramidal needles on a 0.76 cm² round

Table 4
Modified formulations of the SIM NS.

Formulation	N9	N10
Mass of Drug (mg)	100	200
Stabiliser	PVA (9–10 kDa)	PVA (9–10 kDa)
Stabiliser volume (mL)	7	7
Conc. of stabiliser w/w %	1	1

area with a 750 μm needle height, 300 × 300 μm base, and 50 μm interspace, followed by applying a positive pressure of 5 bars for 3 min in a pressure chamber (Richmond Scientific, Chorley, UK). Afterwards, 300 mg of PVA-PVP aqueous solution (1:1 w/w mixture of 30 % w/w PVA 10 kDa and 40 % w/w PVP 58 kDa) was cast on the surface of the mould as the second layer and centrifuged at 3500 rpm for 10 min. Following these, a 3D-printed baseplate was designed to have a round shape with a diameter of 13 mm and a thickness of 0.6 mm and was printed with PLA filaments. It was adhered to the solidified second layer using glue dots. Fig. 2 illustrates the manufacturing process of the trilayer structure.

3.2.4. Characterisation of SIM NCs-loaded DMNs

The characterisation of the mechanical properties, insertion profiles, and drug content of the DMNs followed the same procedures with the EMNs as described in section 3.1.4. To visualise the concentration of SIM NCs in the DMN tips, methylene blue was added to the drug-incorporated first layer formulation for staining. The morphology of the fabricated DMNs was visualised by a Hitachi TM3030 tabletop scanning electron microscopy (SEM) instrument (Chiyoda-ku, Tokyo, Japan) under 150 × and 500 × magnification.

3.3. Ex vivo skin permeation and deposition studies

Ex vivo drug permeation and deposition studies of two DMNs (SIM NCs-loaded DMNs and coarse SIM loaded DMNs) and three EMNs (one PMN and two formulations of EMNs) were evaluated using a Franz cell apparatus. Prior to MN application, the receptor chamber was filled with 12 mL of 1 % w/v SDS in PBS and maintained at 37 °C for at least 30 min. The excised full thickness porcine skins were shaved using a razor and equilibrated in PBS for 30 min. Afterwards, the MNs were manually inserted into full-thickness neonatal porcine skin for 30 s (Li et al., 2022). A 12 g metal weight was then placed on the inserted MNs. At each time points, 200 μL of sample was taken and replaced with 200 μL of fresh medium. The samples were subsequently centrifuged at 14,800 rpm for 10 min to remove impurities. The supernatant was collected and subjected to RP-HPLC to quantify the amount of SIM permeation. After 24 h, the baseplates were removed and the skin samples were collected. The skin surface was carefully cleaned with a damp paper towel to remove the excess formulation and gel residue (Paredes et al., 2021). The skin was observed under the digital light microscope, and the drug deposited in the skin was extracted and quantified using the method developed in section 3.1.6. Formulations with higher permeability and deposition efficiency in each cohort were selected for subsequent *in vivo*
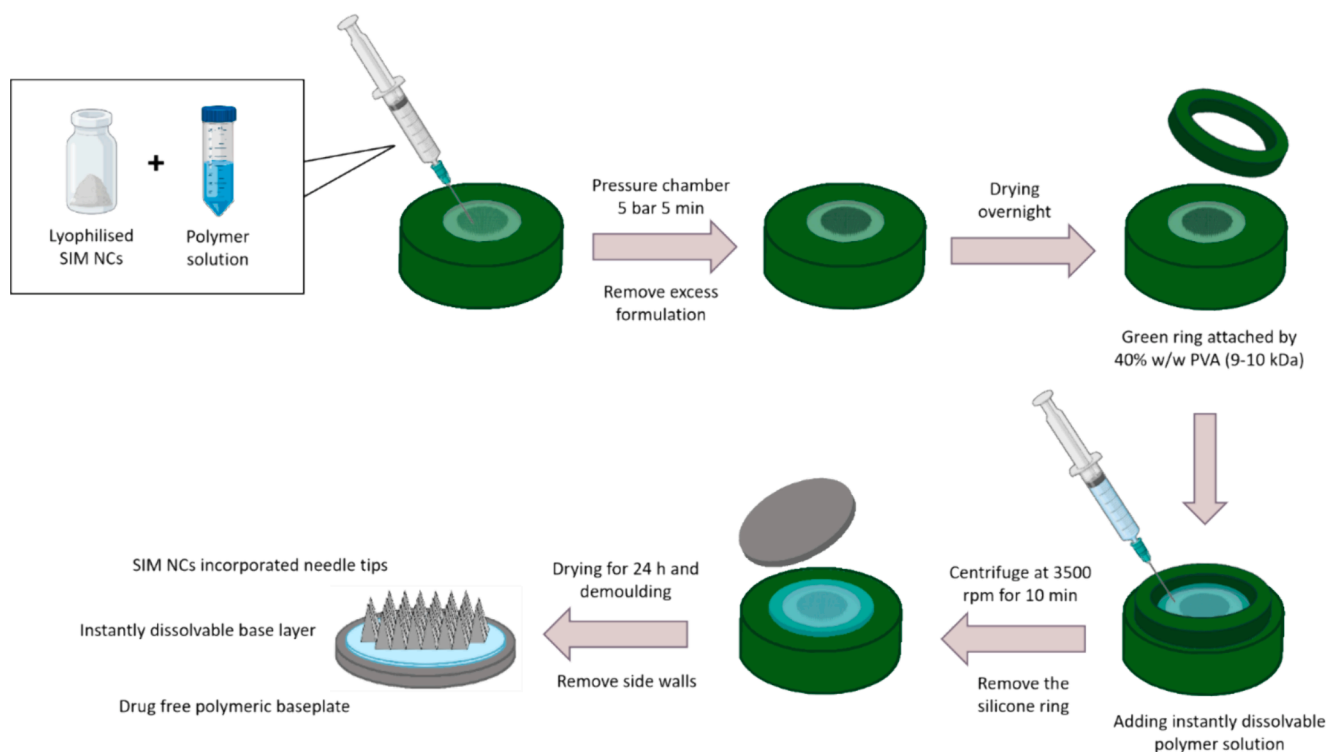
Table 3
Parameters of trials for SIM nanosuspension preparation.

Formulation	N1	N2	N3	N4	N5	N6	N7	N8
Mass of drug (mg)	100	100	100	100	100	100	100	100
Bead diameter (mm)	0.1–0.2	0.1–0.2	0.1–0.2	0.1–0.2	0.1–0.2	0.1–0.2	0.1–0.2	0.1–0.2
Mass of beads (mL, g)	2, 6.9	2, 6.9	2, 6.9	2, 6.9	2, 6.9	2, 6.9	2, 6.9	2, 6.9
Stabiliser	P 188	P 407	T 80	HEC	SLS	MC	PVP	PVA
$V_{stabiliser}$ (mL)	7	7	7	7	7	7	7	7
$C_{stabiliser}$ (w/w %)	2	2	0.5	0.5	1	1	2	2
Stir bar size (mm)	12 × 6	12 × 6	12 × 6	12 × 6	12 × 6	12 × 6	12 × 6	12 × 6
Stir bar quantity	4	4	4	4	4	4	4	4
Rotation speed (rpm)	1500	1500	1500	1500	1500	1500	1500	1500

$V_{stabiliser}$: Stabiliser volume; $C_{stabiliser}$: Concentration of stabiliser aqueous solution

Fig. 2. Schematic representation of the fabrication of SIM NCs-loaded trilayer DMNs with a PLA baseplate.
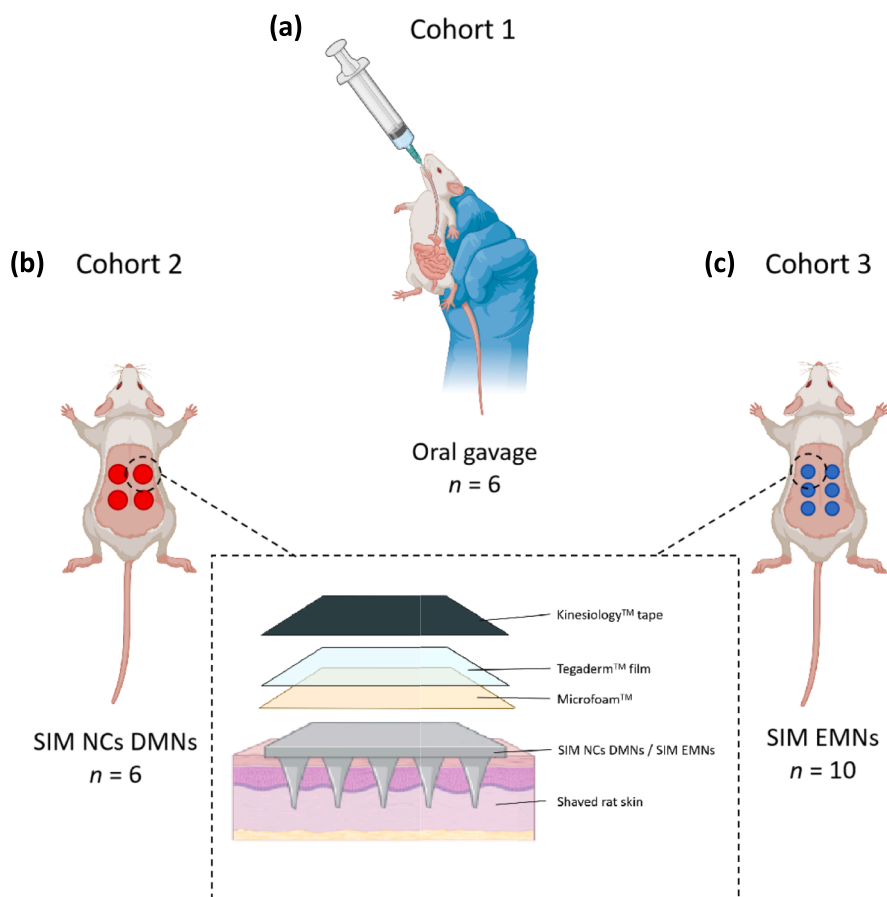

Fig. 3. Schematic representation showing the three cohorts for *in vivo* studies: (a) Oral administration of 16 mg/rat of the SIM suspension. (b) Intradermal application of four SIM NCs loaded DMNs (each patch contained 2.65 mg of SIM). (c) Intradermal application of six SIM EMNs (each patch containing 350 µg of SIM).

experiments.

3.4. Stability of SIM loaded formulations in EMNs and DMNs

Stability of SIM NCs-encapsulated formulation in DMNs and powder formulation in EMNs were evaluated by preparing standards of 10 mg of each formulation in sealed plastic vials. Samples were prepared in triplicate and stored under the ambient temperature (fabrication conditions) and 37 °C (*ex vivo* and *in vivo* conditions). The samples were taken at Day 0, 3, 7, 14, and drug recovery was quantified using HPLC-UV.

3.5. In vivo delivery of SIM from DMNs and EMNs

3.5.1. Preparation of the SIM oral suspension

The mass of SIM required to produce a final suspension with a concentration of 16 mg/mL was accurately weighed. Afterwards, 0.5 % w/w solution of methylcellulose (MC) solution was added to the SIM powder under continuous stirring until a smooth and homogenous suspension was formed. The final suspension was stored at 2——8 °C until use and was prepared approximately 24 h before the *in vivo* experiment.

3.5.2. In vivo evaluation of plasma pharmacokinetics

The *in vivo* delivery of SIM mediated by DMNs and EMNs was investigated by pharmacokinetic and biodistribution studies. The study was carried out in healthy female *Sprague-Dawley* rats (n = 22), with an initial weight of 298.95 ± 43.67 g at the beginning of the experiment. The animals were divided into three cohorts, each consisting of 6, 6, and 10 rats. The first cohort (rats 1–6) served as a control cohort and received 1 mL of an oral aqueous suspension in 0.5 % w/v methylcellulose containing 16 mg of SIM *via* oral gavage, as described in section 3.4.1 (Fig. 3a). The second cohort (rats 7–12) received four SIM NCs-loaded DMNs on the backs of the animals, with a dose of 2.65 mg/patch (Fig. 3b). The final cohort (rats 13–22) received six SIM EMNs at a dose equivalent to 2.58 mg/rat (Fig. 3c). The details are summarised in Table 5. This study was approved by the Committee of the Biological Services Unit (BSU), Queen's University Belfast, under project license PPL 2903 and Procedure Individual License numbers 2127, 2205, 2206 and 1892. Blood samples (100 μL) were collected at pre-determined time points *via* tail vein bleeds into 1.5 mL pre-heparinised tubes (10 μL) over 15 days. The time points were set at 1, 2, 4 and 6 h, and 1, 2, 3, 4, 9 and 15 d after MN application. At 24 h, the baseplates of the MNs were removed under gaseous anaesthesia, and the drug deposition arrays left by the two MN cohorts were observed. Afterwards, four rats in cohort 3 were culled using carbon dioxide (CO_2) asphyxiation and dissected to investigate the ability of SIM EMNs to deposit the skin. Thereafter, blood samples were collected from all rats (n = 18) from 24 h to 15 days.

3.5.3. Sample processing and analyte extraction

Blood samples were centrifuged at 1500 rpm at 4 °C for 10 min to separate the plasma from other components of the blood. To extract the analyte from the obtained plasma, 1 mL of ethyl acetate (EA) was added to each plasma sample (100 μL) in a microtube. The mixture was then vortexed at 1500 rpm for 30 min to achieve adequate extraction and plasma protein precipitation. Following these, the samples were centrifuged at 14,800 rpm at 4 °C for 10 min, after which the supernatants were transferred to disposable glass culture tubes for solvent

evaporation. These were placed into a Zymark TurboVap® LV Evaporator Workstation to vaporise the organic solvent under a nitrogen stream (5 psi) at 37 °C for 40 min. The residues were reconstituted in a 100 μL mixture of mobile phase by vortexing for at least 30 s. Samples were transferred into HPLC vials containing glass inserts (250 μL), followed by quantification using LC-MS.

Skin samples from cohort 3 obtained from dissection were chopped into small pieces along the area where the EMNs were applied and weighed accurately using an analytical balance. Each skin sample was cut into fragments and 0.5 mL of deionised water was added. These were disrupted using the Tissue Lyser for 15 min (50 Hz). Following this, an aliquot of 1 mL ACN was added, and the mixture was homogenised for another 15 min (50 Hz). The obtained blends were centrifuged at 14800 rpm at 4 °C for 10 min, and an aliquot of 100 μL of the supernatant was transferred to a 1.5 mL Eppendorf tube. The subsequent processing procedure was consistent with that used for the plasma samples and were then analysed using LC-MS.

3.5.4. Calculation of pharmacokinetic parameters and relative bioavailability

Non-compartmental pharmacokinetic analysis of the plasma concentration profiles of SIM and SIMA was conducted by PKSolver (Zhang et al., 2010), which is an add-in program of Microsoft Office 365 (Microsoft Corporation, Redmond, WA, USA). The curves of the drug concentration [ng/mL] versus time [h] were plotted for SIM and SIMA. The maximum plasma concentrations (C_{max}) and the times of maximum plasma concentrations (T_{max}) were determined from the raw data. The area under the curve (AUC) from time zero (t = 0) to the endpoint of the experiment (t = 360) was calculated with the linear trapezoidal method using Eq. (6), which was calculated in terms of the mean concentration ($c_1 + c_2$) over the time interval ($t_2 - t_1$). The relative bioavailability (F_{MNs}) of intradermal delivery *via* two types of MNs was calculated by Eq. (7), where F_{MNs} is the bioavailability of intradermal delivery from MNs, and F_{oral} is the oral bioavailability of SIM after oral gavage administration, which was reported to be 5 %. $Dose_{oral}$ and $Dose_{MNs}$ are the amount of SIM given orally and using MNs, respectively, and AUC_{MNs} and AUC_{oral} represent the area under the curve of plasma concentration versus time from t = 0 and t = 360 h in the oral cohort and two MN cohorts, respectively.

$$AUC_{0-360} = \frac{1}{2}(c_1 + c_2)(t_1 - t_2) \tag{6}$$

$$F_{MNs} = F_{oral} \times \frac{AUC_{MNs} \bullet Dose_{oral}}{AUC_{oral} \bullet Dose_{MNs}} \tag{7}$$

3.6. Pharmaceutical analysis

The concentrations of SIM and SIMA for *in vitro* samples were determined *via* HPLC (Agilent Technologies 1220 Infinity UK Ltd, Stockport, UK) combined with UV detection conducted at 240 nm. An Inertsil® C_{18} ODS-3 (250 mm × 4.60 mm, 5 μm packing) was used for separation. The mobile phase consisted of 80:20 % v/v acetonitrile and water/phosphoric acid (0.1 % v/v) (pH=2.24) at a flow rate of 1 mL/min. Column temperature was set at 25 °C and the injection volume was 20 μL. The Agilent ChemStation® Software B.02.01 was used to analyse the chromatograms. The retention time of SIMA and SIM were found at 4.3 min and 6.9 min, respectively. For *in vivo* studies, the analysis of SIM and SIMA in plasma and tissues was performed using the HPLC instrument coupled to a single quadrupole API 6400 mass spectrometer (Agilent Technologies, UK) with electrospray ionisation (ESI). The separation was carried out using the same C_{18} column. The detection was performed in positive mode of ESI for SIMA at *m/z* 435.2 and switched to negative mode for the detection of SIM at *m/z* 419.9 after a running time of 9.5 min. Table 6 summarises the chromatographic conditions for the detection and quantification of *in vivo* samples. The HPLC-MS method

Table 5
Treatment cohorts designed for *in vivo* pharmacokinetic and biodistribution studies.

Treatment cohorts		
Cohort 1	Cohort 2	Cohort 3
Oral SIM suspension (16 mg/rat)	Four SIM NCs loaded DMNs (10.5 mg/rat)	Six SIM loaded EMNs (2.58 mg/rat)

Table 6

Chromatographic conditions for the separation and quantification of SIM and SIMA from *in vivo* sample matrices using HPLC-MS.

Parameter	Condition
Column	Inertsil® C_{18} ODS-3 (250 mm × 4.60 mm, 5 μm packing)
Column temperature [°C]	25
Mobile phase	ACN: Phosphoric acid 0.1 % (80:20 v/v)
Flow rate [mL/min]	1
Injection volume [μL]	30
UV detection wavelength [nm]	240
Retention time [min]	[SIMA] 8.8 min; [SIM] 11.5 min
Run time [min]	9

was validated as per the International Committee on Harmonisation (ICH) 2005.

3.7. Statistical analysis

All the data were calculated using Microsoft Office 365 Excel (Microsoft Corporation, WA, USA) and are expressed as the means ± S.D or means + S.D. Statistical analysis was carried out using GraphPad Prism® 7 (GraphPad Software, San Diego, CA, USA). When necessary, an unpaired *t*-test was used for comparisons of two groups and a one-way ANOVA was used for comparisons among multiple groups. In all cases, $p < 0.05$ indicated statistical significance.

4. Results and discussion

4.1. Effervescent hollow MNs

4.1.1. Characterisation of dissolvable hollow shells

Dissolvable hollow shells were prepared with biodegradable and biocompatible polymers. The aqueous polymer solution in the holes of the moulds gradually formed grooves as the water evaporated and finally generated a solidified shell structure. Size of the moulds (5 × 5 array arranged on a 0.25 cm^2 area, 1.1 mm needle height and 70 μm interspacing) were selected based on ensuring an effective connection between the hollow shells and the baseplate. Such spacing and density of the needles are designed to guarantee a secure connection, allowing for successful powder filling and demoulding without issues such as needle missing. The physical appearance and evaluation of the prepared polymeric shell of EMNs are summarised in Table 7. The properties of polymeric shells are related to the type and degree of polymerisation, as well as the concentration of the polymer. Intuitively, SF3, SF4, SF5 and SF8 seemed to be promising formulations with larger internal hollow volumes, as well as vertical and sharp needle shapes. Furthermore, the equilibrium of the concentration of the polymer solution is crucial. Generally, a more concentrated polymer solution can leave a larger amount of solidified polymer in the tips of MN moulds after the solvent is completely evaporated, resulting in a restricted capacity of the hollow structure. This was previously confirmed in a study by Kim et al. (2020). As the polymer concentration of the shell formulation (CMC) increased from 5 % to 20 %, the size of the microcavities decreased by approximately 60 %. On the other hand, a polymer solution with an excessively low concentration may conversely increase the fluidity of the formulation and reduce the viscosity. The cohesion between the polymer molecules is not sufficient to counteract the gravity on them, thus resulting in the accumulation of polymer and rejection of the formation of shell structures. These findings could explain the smaller microcavity volumes of the first three formulations (SF1-SF3).

Empirically, a larger microcavity represents greater potential for more drug loading. Therefore, loading capacity is characterised by comparing the cavity heights, and a schematic representation of the height of the microcavity is illustrated in Fig. 4a. As stated above, SF1 to

SF3 had significantly smaller cavity heights of 16.20 ± 1.57 %, 35.88 ± 3.66 % and 35.68 ± 2.96 %, respectively, none of which exceeded 40 % (Fig. 4b). The cavity heights of SF4 to SF8 were nearly 80 %, corresponding to a length of nearly 850 μm, which suggested the possibility of higher drug loading and deeper delivery. There was no significant difference between SF4, SF6 and SF8 ($p = 0.886$, $p = 0.067$). An increased microcavity capacity may in turn reduce the robustness (Wang et al., 2016). Therefore, mechanical tests were applied to the hollow shell to ensure sufficient strength to penetrate the *SC* and deliver drug molecules into deeper live tissues without bending or damage (Hardy et al., 2016). Representative graphs of the mechanical properties are shown in Fig. 4c. SF4 and SF8 had weaker needle shell strengths (34.70 ± 3.68 % and 50.65 ± 2.43 %, respectively). SF6 (20 % w/w PVA 31–50 kDa) demonstrated the lowest height reduction of 14.91 ± 1.85 % ($p < 0.0001$, $p = 0.0076$, $p < 0.0001$) compared to the other three formulations. This provided a promising robustness for further insertion.

Upon skin application of EMNs, the shells absorb the interstitial fluid from the skin and gradually dissolve, thereby releasing the internal loaded powder formulation to the microcirculation. Ideally, needle shells have to undergo rapid dissolution, as it signifies quicker contact of the powder formulation with the skin tissues. Moreover, since the effervescent design was introduced into the internal powder formulation in future studies, the function of the effervescent agents may not be fully effective if the polymeric shell dissolves slowly. The dissolution rate of the needle shell formulation is empirically related to the type, concentration and molecular weight of the polymer (Wang et al., 2003). As shown in Fig. 4d, the dissolution rates of SF5 and SF6 were 185.67 ± 6.11 s and 213.67 ± 7.09 s, respectively, which were considered acceptable. In this study, formulations with more robust properties were used to maximise the ability to puncture the skin layer, which was the basis for in-skin delivery. As a result, 20 % w/w PVA (31–50 kDa) was selected as the formulation for subsequent EMN fabrication. The development of conventional DMNs has been restricted by drug hydrophobicity, while the successful preparation of such hollow shells can circumvent the problems in preparation caused by insoluble drugs and hydrophilic backbone matrices.

4.1.2. Characterisation of the SIM EMNs

The height proportion of the filled powder in each needle was evaluated to estimate the insertion depth in skin tissues. All three formulations occupied nearly 70 % of the needle height, and no significant difference was detected (Fig. 4e), indicating a similar insertion depth and contact area. The research conducted by Simões et al. (2018) indicated that SIM exhibits polymorphism in the solid state, with two possible phase transitions occurring at low temperatures, specifically from form III to form II (~232 K) and from form II to form I (~272 K), respectively. Changes in crystalline form can potentially alter the solubility of SIM, thereby influencing the transdermal absorption rate. However, the powder formulations in this study were prepared through physical mixing. The low temperature states above were not involved during the process of fabrication, release study or storage. Consequently, the SIM was in form I (common state) in the powder formulation, where the absorption rate through the skin were not affected by the polymorphism. The addition of effervescent particles did not impact the filling efficiency of the powder formulations into the hollow shell. A compression study of the EMNs revealed that there was no significant difference in the height reduction of the needles among the three formulations after 30 s of manual force on Parafilm M® ($p > 0.05$), with values of 9.46 ± 4.82 %, 9.11 ± 5.00 % and 10.73 ± 4.12 %, respectively (Fig. 4f). The loading of the powder formulation expectedly improved the robustness by dissipating a portion of the pressure that would otherwise be exerted on the needle shell, enabling the powder and the needle shell to be stressed as an entirety. This is similar to the results obtained by Kim et al. (2019). The penetration depth of the needles was also simulated by the Parafilm M® model to determine the insertion capability of the EMN arrays in the skin by observing the
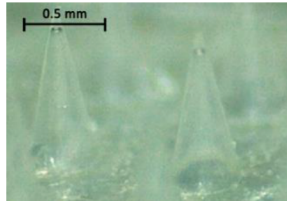
Table 7
Physical properties and morphology of the selected dissolvable shell.

Shell formulation	Aqueous blends	Morphology	Description
SF1	40 % PVP (58 kDa)		Needles were not vertical, very fragile, very little cavity
SF2	20 % PVP (58 kDa)		Needles were not vertical, not sharp, very little cavity
SF3	30 % PVA (9–10 kDa)		Needles were sharp but very little cavity
SF4	20 % PVA (9–10 kDa)		Large cavity but needles were unsubstantial and soft
SF5	20 % PVA (31–50 kDa) & 20 % PVP (58 kDa)		Needles were vertical, sharp, with large cavity
SF6	20 % PVA (31–50 kDa)		Needles were vertical, tough, and very large cavity
SF7	10 % CMC		Shell cavity cannot be formed. Most needles were broken.

Table 7 (*continued*)

Shell formulation	Aqueous blends	Morphology	Description
SF8	5 % HEC		Large cavity but soft needles

number of needle holes created in each layer. All three EMNs presented the ability to penetrate six or more layers of Parafilm M® (>750 μm) under manual force (Fig. 4g), indicating that more than 70 % of the needle length will be inserted into the skin. The thickness of the epidermis is approximately 150–200 μm, and that of the dermis is approximately 1.1–2.3 mm (Kolarsick et al., 2011; Pailler-Mattei et al., 2008), suggesting that all three EMNs are able to break the *SC* barrier (10 μm) and penetrate the entire epidermis and part of the dermis, thus allowing the delivery of drug molecules to deeper viable cells. Additionally, from the OCT diagram (Fig. 4h), the powder-filled needle was inserted entirely and penetrated 4 layers of Parafilm M®. It is difficult to observe the needle tips in the OCT graph because of the limited length of the laser beam (Li et al., 2022). The needle tips were blunted by pressure after insertion; however, all the needles were still vertical and integral (Fig. 4i). This indicated that the horizontal support of the EMNs was sufficient to allow them to be inserted into the skin. As shown in Fig. 4j, no significant difference was found between the skin and control groups ($p = 0.3278$), indicating that there were no interactions between the skin and SIM. The extraction efficiency of SIM from skin was 98.10 ± 3.23 %, which proved that the extraction method used was effective for subsequent in-skin deposition studies. The drug loadings of the three EMNs are shown in Fig. 4k and were 512.64 ± 5.43 μg, 327.25 ± 40.09 μg and 213.63 ± 56.32 μg for F1-F3, respectively. These results illustrated an inverse relationship between the drug loading and the effervescent content. As the effervescent dose of the formulation increases, the drug loading is affected. As shown in the micrographs in Fig. 5, F1, F2 and F3 all exhibited sharp and clear needle tips with smooth shell surfaces. The EMN arrays containing the three different formulations can be demoulded intact from the mould without cracked or missing tips. The powder formulations filled in the needle shells occupied the majority of the capacity of the shell structures. Each EMN array contained 25 needles with a height of 1.1 mm and an area of 0.25 cm^2.

4.1.3. Ex vivo skin permeation and deposition studies

The *ex vivo* drug permeation and skin deposition performance of the EMNs were assessed using full-thickness excised porcine skin to simulate human skin. After 24 h, all three EMNs were observed to separate from the 3D-printed baseplate and leave depots in the skin (Fig. 6a). These properties provide the provided potential for prolonged release of SIM. Depots left on the skin by F1 appeared to be compact blocks, while the drug depots of F2 and F3 became progressively less evident as the amount of effervescent agent increased. This probably reflected that agglomerated drug particles were distributed more broadly and homogeneously in the skin *via* the assistance of carbon dioxide generated by the effervescent agents, resulting in a more dispersed drug reservoir beneath the skin. As seen in the release profiles of four formulations (Fig. 6b), SIM permeation from the three EMN formulations at 24 h was 15.48 ± 3.49 μg, 29.09 ± 7.45 μg and 22.17 ± 7.62 μg, respectively. Considering drug loading, the presence of effervescent formulations appears to enhance the permeability of poorly soluble drugs to varying degrees, where the permeation efficiencies of F2 and F3 were 10.38 ± 6.70 % and 8.89 ± 2.28 %, respectively. These values were significantly greater than that of F1 (crude SIM-loaded PMNs) ($p = 0.029$; $p = 0.043$, respectively). This can potentially be due to the carbon dioxide

produced that dispersed the compact drug depot after insertion, leading to a larger surface area of contact between the SIM particles and skin. Therefore, more drug particles permeated into the subcutaneous circulation. Another possible reason is that the addition of the effervescent agent might enhance the driving force for molecule penetration. The mechanical motion of the particles it triggered facilitated drug permeation into the hair follicles and skin, which depended on the intensity of the effervescent reaction provided by the formulation (Pereira et al., 2017). This provides the feasibility of enhanced permeation for hydrophobic drugs.

As seen from the results of skin deposition (Fig. 6c), the three EMN array patches F1, F2 and F3 deposited 145.56 ± 25.62 μg, 181.44 ± 19.52 μg, and 113.78 ± 11.45 μg of SIM in the skin, respectively. The actual deposition efficiency of F1 in porcine skin was significantly lower than that of the other two formulations ($p = 0.0139$, $p = 0.0310$) (Fig. 6d). This is closely related to the detachment of the powder-loaded tips from the baseplate. Fig. 9d reveals that when the baseplate of the F1 MN arrays was removed from porcine skin at 24 h, a significant amount of bulky drug depots adhered tightly to the baseplate, leading to a waste of deposited drug and a reduction in the overall deposition efficiency. After application to skin, the effervescent agents loaded in the needle shell react with the interstitial fluid and form the carbon dioxide, which can weaken baseplate attachment to the powder-laden needles and enable separation. This separation principle is comparable with Li et al. (2019), who succeeded in shortening the separation time by introducing an additional effervescent layer between the back layer with the drug-containing needle tips. Also, the bubble generation may break up tightly agglomerated coarse drug powders and increase the wettability of the particle surface to promote dissolution at the junctions of baseplate and needles, which in turn leads to separation. As shown in Fig. 6d, no drug residue remained on the baseplate after F2 EMN was applied for 24 h. Less SIM was wasted after administration, and the deposition efficiency, therefore, significantly improved. The reason for the high accumulation of SIM in the skin is related to the poor solubility. After application to skin, SIM particles are deposited in the aqueous environment of the viable skin layer, where they dissolve slowly and are then absorbed, resulting in a long-acting effect. Similar researches in many commercial NC long-acting drug delivery systems, including rilpivirine, cabotegravir and bictegravir, have been published before (Ramöller et al., 2024; Zhang et al., 2023b). In terms of total delivery efficiency, both F2 and F3 had significantly greater total delivery efficiency than F1 ($p < 0.05$). There was no significant difference in total delivery efficiency between F2 and F3 ($p > 0.05$), while F2 had a greater drug loading than F3. Therefore, F2 (50 % w/w SIM content in powder formulation) was selected as the final EMN formulation and will be applied in future studies to evaluate its *in vivo* performance.

4.2. Dissolving MNs

4.2.1. Rationalisation of SIM NCs

The expansion of the specific surface area of NCs increases the surface free energy, resulting in the spontaneous aggregation of the NCs (Müller et al., 2011). Particle aggregation can be suppressed by selecting appropriate stabilisers. Fig. 7a and b shows that under the same milling
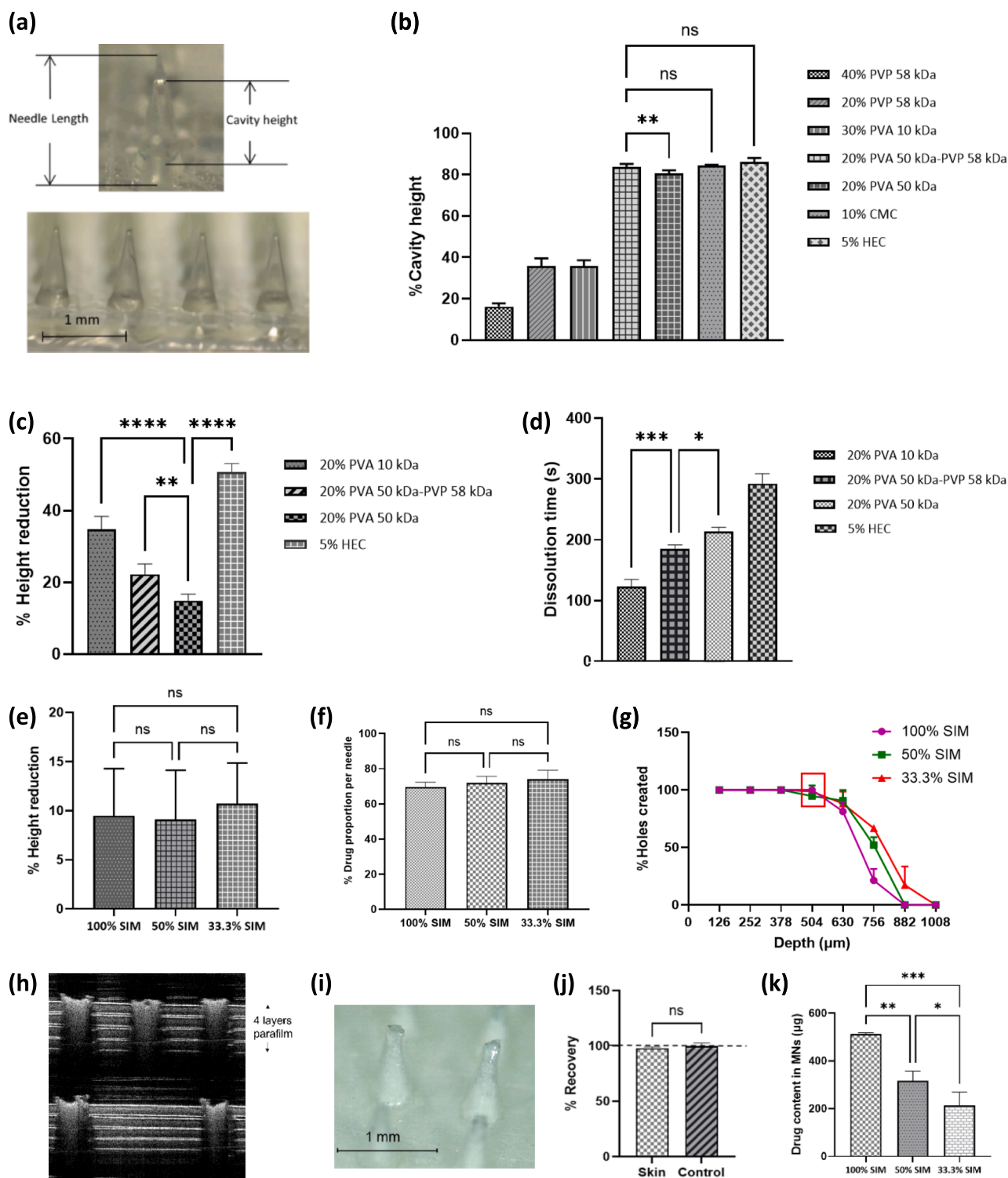
Fig. 4. (a) Schematic representation of the height of the microcavity. (b) Height proportion of the cavity per needle for each formulation (means + S.D., n = 3). (c) Height reduction of the dissolvable shell after applying the hollow shells on 8 layers of Parafilm M® sheets by manual force (means + S.D., n = 4). (d) Dissolution time of the hollow shells in 10 mL of PBS (pH=7.4) with 1 % SDS (means + S.D., n = 3). (e) Height proportion of the filled powder formulation in the three EMNs (means + S.D., n = 5). (f) Reduction in the height of three EMNs after inserted into the 8-layer Parafilm M® (means + S.D., n = 5). (g) Insertion profile of 3 EMN arrays applied to 8 layers of Parafilm M® (means ± S.D., n = 3). (h) Insertion diagram of EMN arrays on Parafilm M® observed by OCT. (i) Morphology of EMN arrays after insertion in 8 layers of Parafilm M® observed by optical microscopy. (j) Mean extraction efficiency and stability of powder formulations in skin tissue fragments (*p* > 0.05) (means + S.D., n = 3). (k) Mean drug content of three EMN formulations (means + S.D., n = 3).
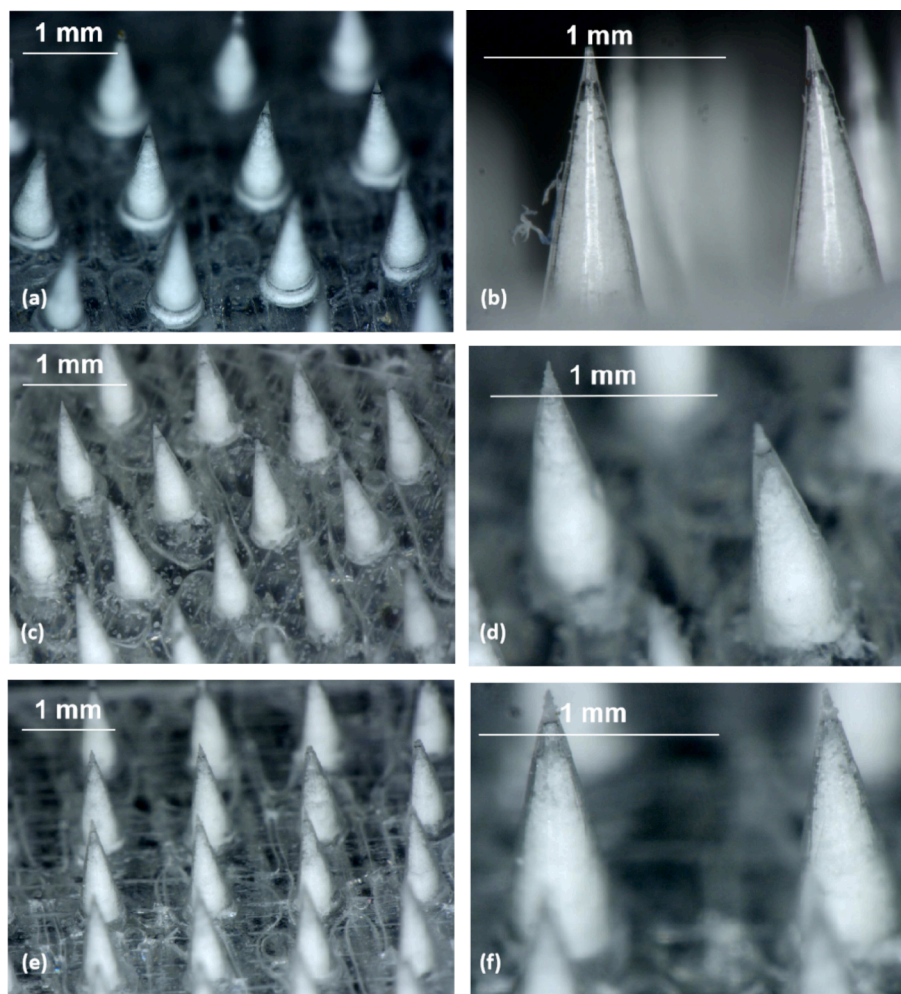
Fig. 5. Micrographs of SIM EMN arrays of F1 (a) and (b), F2 (c) and (d), F3 (e) and (f) taken by digital light microscopy.

parameters, different surfactants and polymers reduced the particle size and PDI with different trends, velocities and magnitudes. In the milling system, aqueous suspensions of drugs and stabilisers were agitated with abrasive beads made of ceramic (Malamatari et al., 2018). With the increasing agitating time, beads and drug particles collide with each other and with the milling chamber, resulting in a gradual reduction of particle size and a stable suspension system under the presence of stabilisers (Afolabi et al., 2014). The particle size and PDI of N8 (2 % w/w PVA 9–10 kDa) were 259.07 ± 1.27 nm and 0.11 ± 0.03 at 24 h, respectively. As one of the most commonly used stabilisers, PVA can attach to the surface of NCs to form a stabilising layer, but also provide a cryoprotectant effect (Kaur et al., 2016), which is crucial to this work, since NCs were freeze-dried in further steps. With respect to the milling time point of N8, no significant difference was found in the particle size between 9 h and 24 h ($p = 0.0750$), whereas there was a greater reduction in comparison to the initial milling stage ($p < 0.0001$), which indicated that the particle size reached the critical threshold at this milling time. Moreover, the PDI value was significantly lower than the previous time point ($p < 0.05$). The shear stress increased in the milling system, and the particle size gradually decreased with prolonged milling time in most of the formulations (Malamatari et al., 2018; Plakkot et al., 2011). However, significant particle growth was observed in N7 at the end of milling in comparison to the initial stage ($p < 0.0001$). This was probably due to the Ostwald ripening caused by the inappropriate stabiliser concentrations (Li et al., 2021). The particle size distribution results are presented in Fig. 7c. The three main parameters of the SIM distributions (Dv10, Dv50 and Dv90) are 2.40, 11.30, and 57.10,

respectively, which implies that 90 %, 50 % and 10 % of the particles in the dispersion system are equal to or less than that value. The particle size of the coarse SIM was 11.30 μm. As per the promising particle distribution performance, 2 % P-188, 2 % P-407, 0.5 % T-80, 1 % SDS and 2 % PVA 10 kDa were selected as the stabilisers for following NCs fabrication. Normally, lyophilisation is an industrial process that involves multiple physical changes during continuous water removal, which can introduce several stresses, leading to colloidal instability, especially the aggregation of particles (Trenkenschuh and Friess, 2021). In the absence of cryoprotectants or lyoprotectants, stability of NCs during lyophilisation is only ensured by their stabilisers (Abdelwahed et al., 2006). As shown in Fig. 7d and e, after a 25-h lyophilisation process, the particle size and PDI of most formulations exhibited apparent particle growth and PDI increase (N1, N2 and N5) ($p < 0.05$). In particular, for N4, the specific particle size and PDI could not be measured after reconstitution, as the particle distribution exceeded the micron level. Fig. 7f shows the morphology of lyophilised NS after reconstitution. Only N8 provided a homogenous and stable suspension after reconstitution without apparent particle agglomeration. As a result, PVA 9–10 kDa was determined to be the stabiliser.

Due to the limited mould-filling capacity of dissolving MNs in future research, the drug loading efficiency of NCs should be prioritised. The theoretical drug loading of N8 was calculated to be 35.7 %. Based on that, drug loading of N9 and N10 was rationalised to be 58.8 % and 74.1 %, respectively, which was improved by increasing the drug proportion and decreasing the amount of the selected stabilisers. The particle size and PDI of three formulations (N8, N9 and N10) before and after the
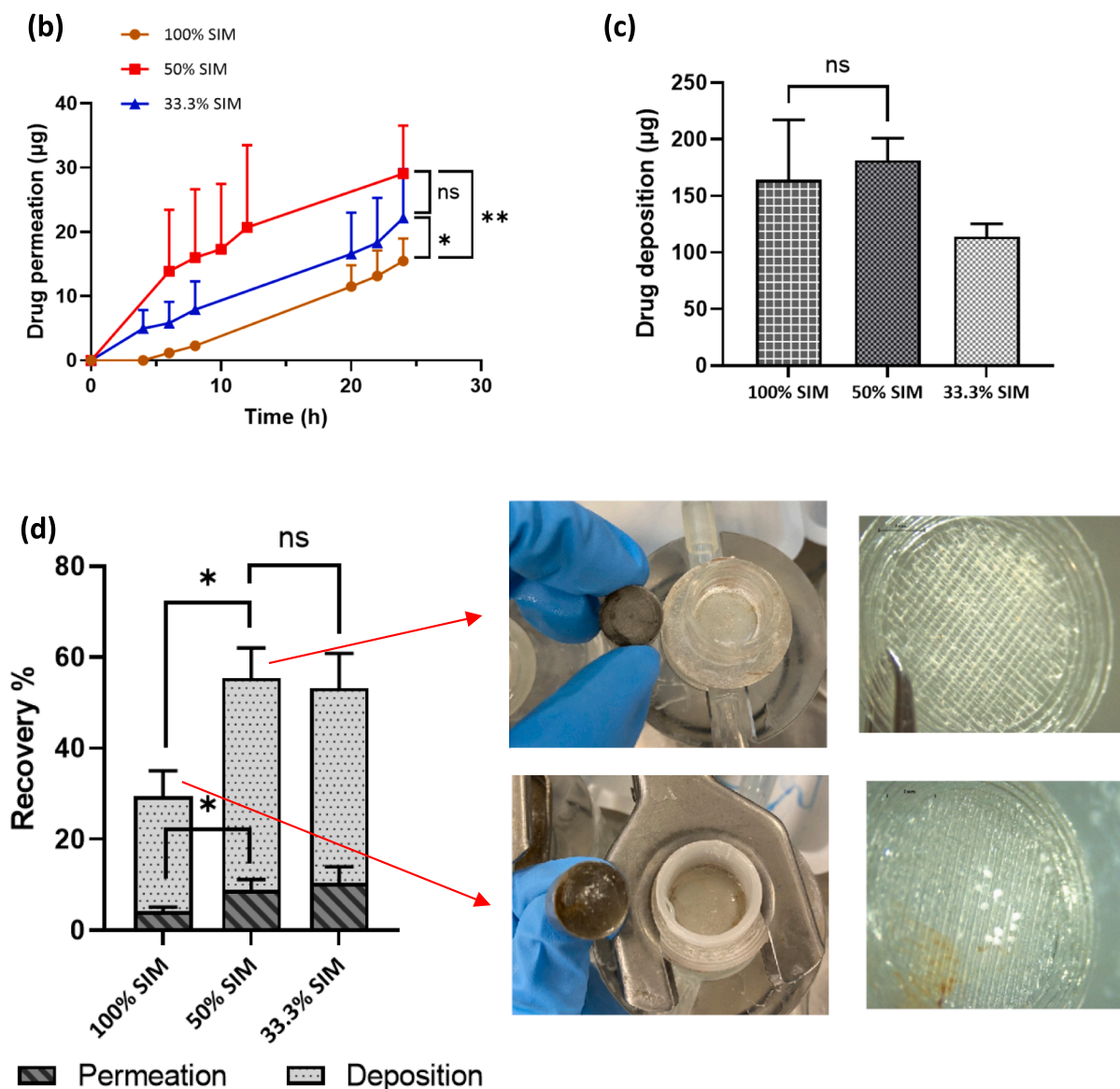
Fig. 6. (a) Observation of full-thickness skin after applying the three EMNs for 24 h. (b) Drug permeation profiles of one PMN (F1) and two EMNs (F2-F3) evaluated by a Franz cell apparatus using full-thickness neonatal porcine skin within 24 h (means + S.D., n = 3). (c) Drug deposition in the skin of three EMNs (means + S.D., n = 3). (d) *Ex vivo* permeation and deposition efficiency of three EMNs (means + S.D., n = 3) with a schematic representation of the drug residue on the PLA baseplate after 24 h.

lyophilisation process were characterised and compared to ensure there was no significant effect on stability when reducing the proportion of stabiliser in the NC composition (Fig. 7g and h). Despite slight particle growth, the particle size and PDI were 296.84 ± 2.15 nm and 0.15 ± 0.01, respectively, after lyophilisation, which was considered acceptable. The final characteristics of the enhanced SIM NC formulation are summarised in Table 8, where an ideal drug loading efficiency is provided. As a result, N10 (1 % PVA 10 kDa, 74.1 % theoretical drug loading) was chosen as the final formulation for DMN fabrication. When fabricating the DMNs, NCs-encapsulated formulation could lead to a more cumbersome preparing process compared to the crude drug loaded MNs. However, the solubility enhancement technique is essential in this project to overcome the dissolution issues.

4.2.2. Fabrication and characterisation of SIM NCs-loaded DMNs

The construction of the trilayer DMNs is displayed in Fig. 8a. The morphology of the SIM NCs-loaded DMNs showed that the blue area

(methyl blue), which is also considered the drug-encapsulated formulation, was highly concentrated at the top of the needle tips (Fig. 8b and 8c). Such a drug distribution can potentially improve the intradermal delivery efficiency and minimised drug waste beyond the skin. The coarse SIM DMNs, on the other hand, display an inhomogeneous drug distribution, where the darker needles are possibly the result of particle agglomeration (Fig. 8d and e). To visualise the particle distribution in the needle tips more clearly, two DMNs were observed using SEM (Fig. 8f-i). The surface of the SIM NCs-loaded DMNs was flat and smooth. The crude SIM-loaded DMNs possessed a rough surface.

As displayed in Fig. 9a, there was no significant difference in the height reduction percentage of the two DMNs following the compression test ($p > 0.05$), which were 5.05 ± 1.14 % and 5.49 ± 1.19 %, respectively. This result is in close agreement with those of previous works of less than 10 % (Zhang et al., 2023b). Both DMNs potentially possess sufficient mechanical properties to penetrate the skin. For insertion studies, two DMNs penetrated three or more layers of Parafilm®M (126
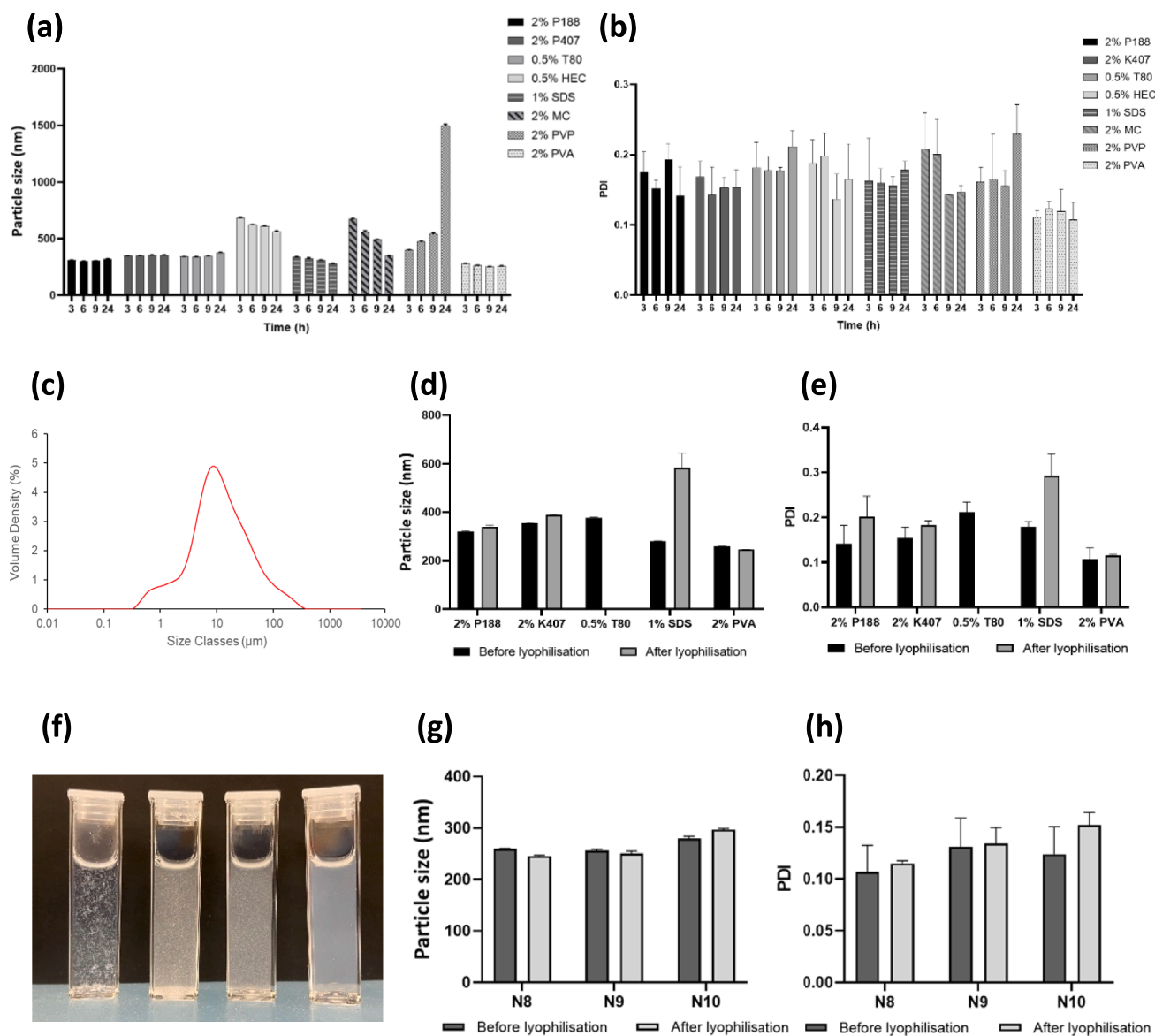
Fig. 7. Mean particle size (a) and PDI (b) of the SIM nanosuspension measured at 4 time points (3, 6, 9 and 24 h) using eight different surfactants and polymers (means + S.D., n = 3). (c) representative size distribution of coarse SIM measured by laser diffraction. Mean particle size (d) and PDI (e) of the SIM NCs before and after the lyophilisation (means + S.D., n = 3). (f) Suspension morphology of NCs after reconstitution by deionised water, where from left to right are formulations of 0.5 % HEC, 0.5 % Tween 80, 1 % SDS and 2 % PVA 10 kDa. (g) Mean particle size and (h) PDI of the N8, N9 and N10 before and after the lyophilisation (means + S. D., n = 3).

Table 8
Primary properties of the fabricated SIM NCs production (mean ± S.D., n = 3).

Particle size (nm)	PDI	Theoretical drug loading (% w/w)	Zeta potential (mV)	Practical drug loading (% w/w)
296.84 ± 2.15	0.15 ± 0.01	74.07	−14.91 ± 0.36	69.83 ± 0.85

μm/sheet), which was equivalent to 50 % of the needle height (Fig. 9b). The percentage of holes created by NCs-loaded DMNs and coarse SIM DMNs on the third layer of Parafilm®M were 20.94 ± 1.92 % and 17.79 ± 6.50 %, respectively. Quantification of the drug from the DMNs was achieved by RP-HPLC. The drug content of the two DMNs were 2.65 ± 0.11 mg/patch and 2.75 ± 0.63 mg/patch, respectively. Although no significant difference was found between the two groups, the results of

coarse SIM DMNs possessed a larger individual differences, as shown Fig. 9c (S.D. = 625.17 μg/patch). The high hydrophobicity of the crude SIM powder resulted in the inhomogeneous distribution of the drug formulation, where sedimentation and delamination might occur when casting the first layer of DMNs (Vora et al., 2018). This could be further confirmed by the micrograph of the MN moulds in Fig. 9d and e, where the nanoformulation was distributed homogeneously in the needle holes of the MN moulds. In contrast, the needle holes of the crude drug DMN were observed with varying shades, indicating an uneven distribution of the drug-encapsulated layer. Furthermore, cross-sectional representative images of SIM NCs-loaded DMNs after insertion into the excised full-thickness porcine skin and Parafilm®M visualised by OCT are displayed in Fig. 9f and g. These results were consistent with those of the insertion study, where the DMNs penetrated 3 layers of Parafilm®M as shown in the OCT images (378 μm). Additionally, DMNs demonstrated ideal insertion ability in full-thickness porcine skin, with the white portion of
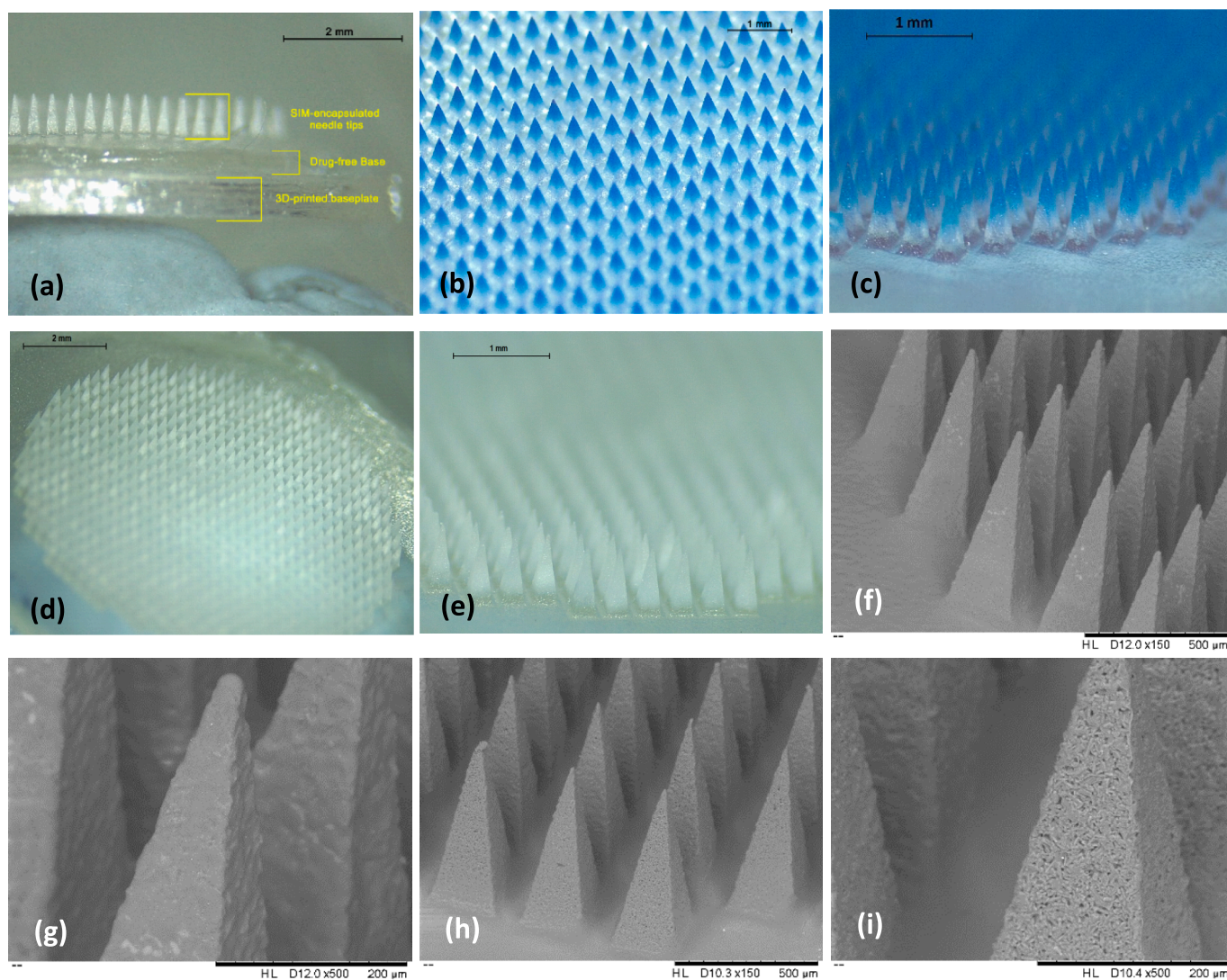
Fig. 8. (a) Micrographs of trilayer structure SIM NCs-loaded DMNs with a drug encapsulated layer, a drug-free dissolvable base layer and a 3D-printed baseplate. Representative micrographs of (b) and (c) SIM NCs-loaded DMNs with methylene blue as a dye. Micrographs of (d) and (e) crude SIM loaded DMNs. SEM images of (f) and (g) SIM NCs-loaded DMNs and (h) and (i) crude SIM loaded DMNs.

the drug-encapsulated needle tips entirely deposited in the skin, providing efficient drug delivery potential. In both temperature conditions, drug formulation of two MNs were stable for at least 14 days (Fig. 9h). Drug recovery percentage ranged between 99.72 % to 101.31 % for DMNs and 99.86 % to 100.96 % for EMNs, which confirms the stability during the entire period of study.

4.2.3. Ex vivo skin deposition and permeation study of DMNs

After 24 h, the baseplates of two DMNs were removed from the porcine skin, and the white drug reservoir was observed under a digital light microscope (Fig. 10a and b). These factors provided the potential for the sustained release of SIM. The amount of drug depots left by the crude SIM DMNs was not as obvious as that left by the SIM NCs DMNs after 24 h. Drug permeation at various time points was evaluated, and the results are shown in Fig. 10c. The SIM NCs DMNs demonstrated enhanced drug permeability, with a cumulative release amount of 406.67 ± 41.38 μg at 24 h, which was significantly greater than that of the crude SIM DMNs (246.69 ± 52.49 μg; $p = 0.0076$). This can be attributed to the high dissolution rate of NCs. Two DMNs still displayed a continued release tendency in 24 h, and the subsequent sustained drug permeation was supported by the drug reservoirs deposited in the skin. The amount of drug deposited by SIM NCs DMNs was 656.73 ± 100.76

μg/patch, which was significantly greater than the crude SIM DMNs ($p = 0.009$), indicating a relatively prolonged release potential (Fig. 10d). The higher deposition efficiency is potentially due to the greater contact area that NCs provide with the skin, which promotes interaction and absorption, improving the capacity for the skin deposition (Yu et al., 2021). Fig. 10e shows that the amount of drug permeation increased gradually as the deposition content progressively decreased over time. As per the results obtained above, total delivery efficiency of SIM NCs loaded DMNs was 40.11 ± 4.53 % than that of crude SIM DMNs 21.93 ± 3.87 % ($p = 0.0062$) (Fig. 10f). The *ex vivo* results of NCs loaded DMNs were supposed to be a reference for the *in vivo* dosage calculations.

4.3. In vivo delivery of SIM from DMNs and EMNs

After applying the MNs for 24 h, the depots left by MNs on the skin were clearly visible, as shown in Fig. 11. The intermediate base layer of DMNs was fully dissolved and white blocky depots were left in the skin (Fig. 11a). There were no visible drug or polymer residues remaining on the baseplates (Fig. 11b and c). For the EMNs, clear imprints of needle arrays remained on the surface of the skin (Fig. 11d). The baseplates of the EMNs were fully separated with needle tips and no bulky powder depot was attached on the baseplates (Fig. 11e and f), which further
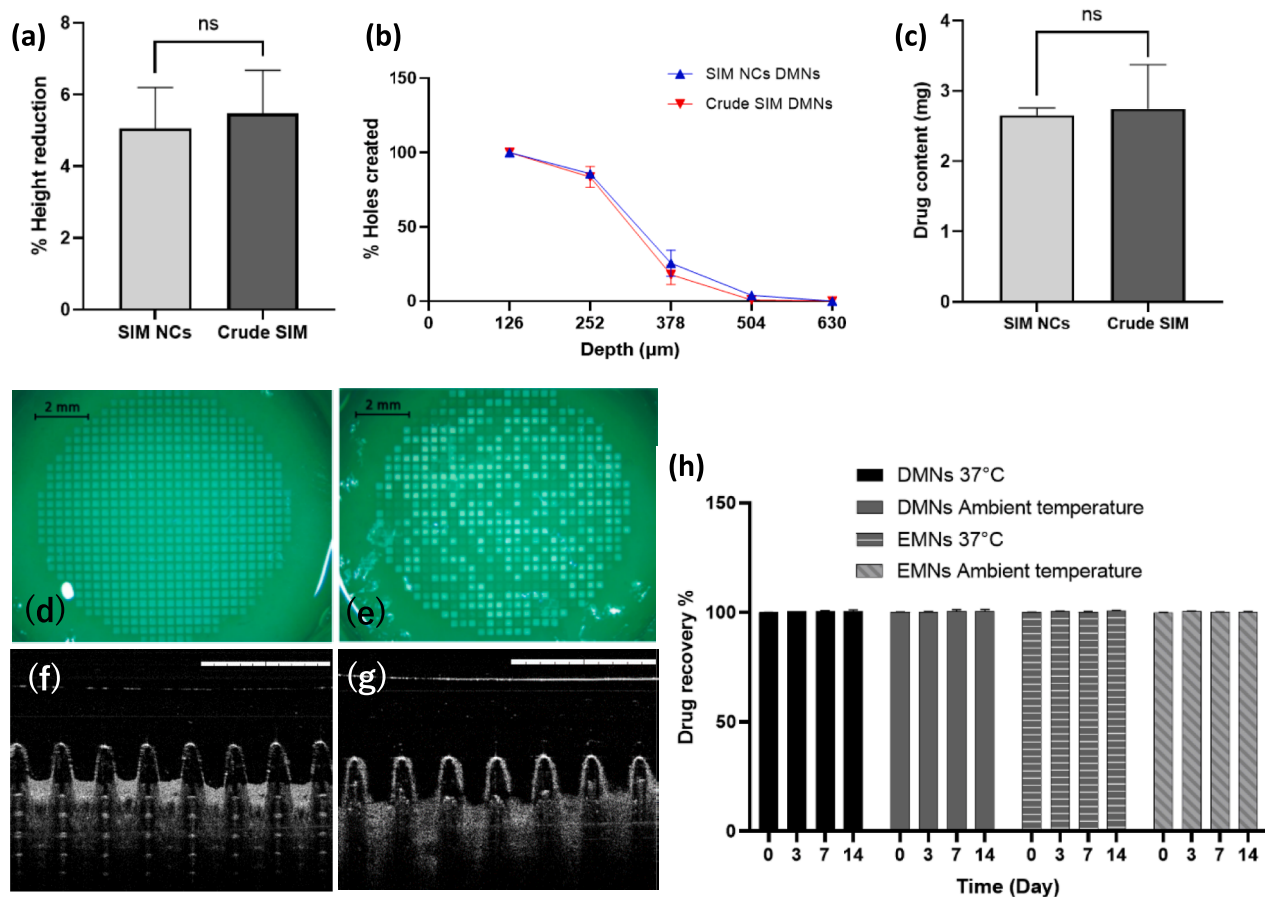
Fig. 9. (a) Comparison of the percentage of height reduction of SIM NCs-loaded DMNs and crude SIM DMNs (means + S.D., n = 5). (b) Insertion profile of two DMNs applied to 8 layers of Parafilm M® (means ± S.D., n = 4). (c) Mean drug loading of two DMNs (means + S.D., n = 3). Schematic representation of the first layer distribution of (d) nanoformulations and (e) coarse SIM formulations in MN moulds. Representative OCT images of the SIM NCs-loaded DMNs inserted into (f) Parafilm® M and (g) porcine skin. The scale bar represents a length of 1 mm. (h) Stability of formulations in DMNs and EMNs under different conditions up to 7 days (means + S.D., n = 3).

verified the addition of effervescent agent can potentially improve the drug distribution and needle separation. There were no large, undissolved drug particles observed on the skin in both cohorts.

According to previous studies, SIM undergoes rapid metabolism *in vivo* to the active simvastatin hydroxy acid (SIMA). Therefore, the plasma profiles of both SIM and SIMA were studied. A summary of the mean pharmacokinetic parameters obtained from the plasma samples is given in Tables 9 and 10. The mean plasma concentration and time profiles after oral gavage, SIM NCs DMN and SIM EMN application are presented in Fig. 12a and b. In the control cohort, SIMA showed a C_{max} of 1278.26 ± 471.25 ng/ml within 1 h and SIM had a C_{max} of 220.66 ± 172.96 ng/ml within 2 h, respectively. This result was comparable to the results obtained by Liu et al. (2015) after the oral administration of 40 mg/kg SIM to rats. In their research, most of the SIM was similarly converted to its active product SIMA. In the DMN cohort, SIMA had a C_{max} of 228.72 ± 75.35 ng/ml within 2 h and 120.71 ± 76.97 ng/ml within 24 h for SIM. For EMN cohort, the C_{max} of SIMA is 59.33 ± 6.32 ng/ml at 4 h and the C_{max} of SIM is 150.25 ± 13.32 ng/ml at 24 h. Statistically, the C_{max} of SIMA after oral administration were significantly higher than that of the MN cohorts ($p = 0.062$, $p = 0.030$). In the profile of oral cohort, plasma concentrations of SIM and SIMA present an abrupt increase to the peak followed by a rapid clearance below the lower limit of quantification (LLOQ) (14.24 ng/ml, 11.54 ng/ml) within 24 h. In contrast, both SIM and SIMA presented relatively smooth, constant, and prolonged plasma concentration profiles with less

pronounced C_{max} after MN administration. Presently, simvastatin taken orally is concomitantly associated with non-negligible negative side effects (Sinzinger et al., 2002), particularly the muscular toxicity of statins, which is a dose- and concentration-dependent phenomenon (Yebyo et al., 2019), and the risk of toxicity increases along with the plasma concentrations (Filppula et al., 2021). As a result, a reduced C_{max} of SIM/SIMA might reduce the toxic side effects caused by the high peak concentration (Ward et al., 2019). Moreover, the sustained release characteristics of plasma profile (including a prolonged T_{max} and larger AUC) indicate the long-term effects of MN administration (Ahmad et al., 2023). After the application of the DMNs and EMNs, plasma concentrations of both SIM and SIMA were found to be above the LLOQ for 9–15 days. Interestingly, the application of EMNs appeared to retard the rate of conversion of SIM to its active form SIMA, where SIM was more present in its lactone form in rats, with a significantly larger AUC of 12764.95 ± 7146.89 ng/ml*h despite the lower administration dose ($p = 0.0468$). This might be related to the powder administration of SIM by EMNs. However, whether the ability of sustained drug delivery was affected by the interconversion of SIM and SIMA was not comparable due to differences in the dose and type of MNs. As a consequence, to facilitate a more comprehensive comparison of the overall delivery situation and calculate accurate relative bioavailability, mathematical integration was considered for the two sets of data, where the SIMA in each set of data was equivalently converted back to SIM using Eqs. (8) and (9). The resulting equivalent pharmacokinetic parameters are
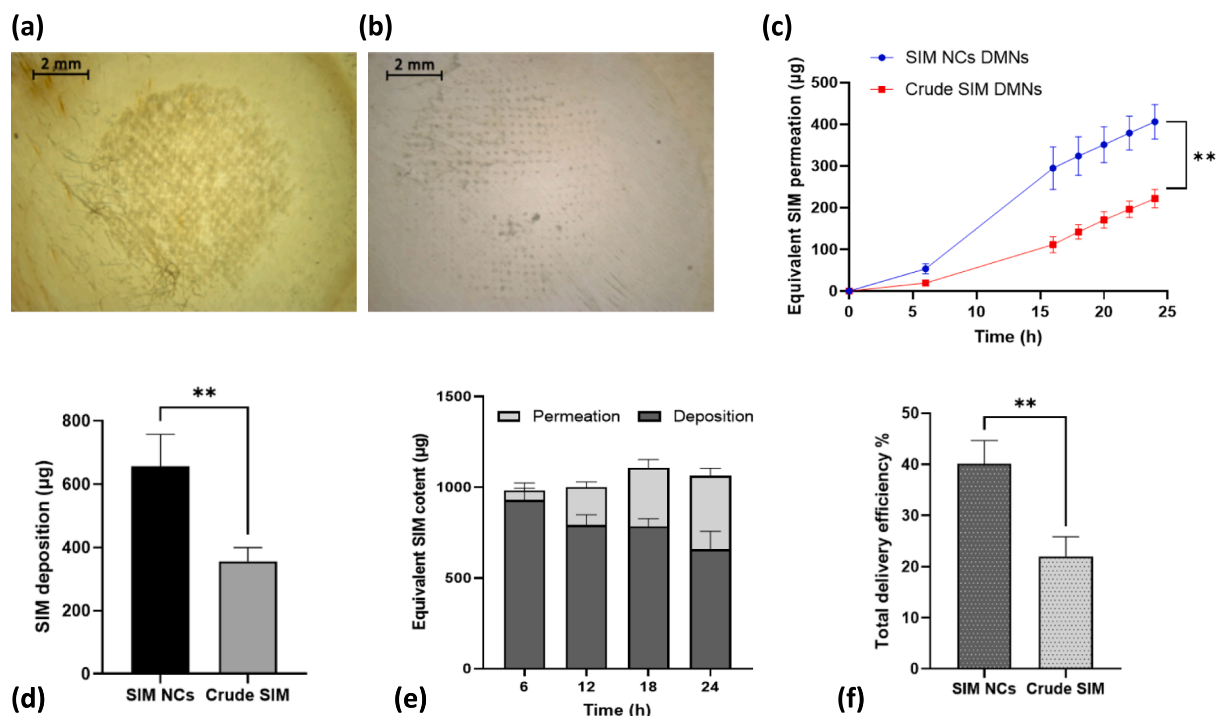
Fig. 10. Representative light microscopy images of skin samples after applying (a) SIM NCs loaded DMNs and (b) crude SIM DMNs for 24 h observed under the transmitted light. (c) Drug permeation across the full-thickness skin of two DMNs within 24 h (means ± S.D., n = 3). (d) Skin deposition after 24 h using a Franz cell model (means + S.D., n = 3). (e) Cumulative amount of SIM deposited and permeated from SIM NCs loaded DMNs at different time points (6 h, 12 h, 18 h, and 24 h) (means + S.D., n = 3). (f) Total delivery efficiency of two DMNs (means + S.D., n = 3).

summarised in Table 11 and the *in vivo* plasma profile of the equivalent SIM plasma concentration is displayed in Fig. 12c.

$$\text{Equivalent SIM content} = \frac{\text{SIMA content}}{\text{Mw}_{\text{SIMA}}} \times \text{Mw}_{\text{SIM}} \quad (8)$$

Backman et al. (2000) reported a maximum plasma concentration of 6.87 ± 3.30 ng/ml after oral administration of 40 mg of SIM to ten healthy human volunteers. In this study, the equivalent SIM plasma concentration was consistently higher than that value within 15 days after application of two MN cohorts, which were 14.63 ± 13.86 ng/ml and 15.50 ± 15.33 ng/ml at the 15 days, respectively. Furthermore, the plasma profiles of the EMN cohorts were smoother and more stable without erupting concentration increase. In addition, the DMNs and EMNs exhibited progressively prolonged T_{max} and increased AUC, respectively, implying sustained release characteristics. According to previous literature, the oral bioavailability of SIM is approximately 5 % (Moon et al., 2017). Based on the pharmacokinetic parameters, the relative bioavailabilities of DMNs and EMNs were calculated to be 24.28 % ± 1.49 % and 103.82 % ± 21.69 %, respectively. The results revealed that SIM NCs-loaded DMNs and SIM EMNs improved the bioavailability of SIM to varying extents in comparison with the conventional oral delivery route. In particular, the relative bioavailability of SIM EMNs was greater than 100 %, suggesting that this novel intradermal delivery system provides more efficient delivery and greater *in vivo* absorption. At 24 h of the *in vivo* study, four rats in the SIM EMN cohort were culled

to evaluate in-skin deposition performance. The total amount of SIM deposited in the dorsal skin of the rats was 11094.79 ± 4712.48 ng/g, which is similar to the results of the *ex vivo* permeation study, where most of the SIM was deposited in the skin as a prerequisite for the sustained intradermal delivery. This confirmed the authenticity of the ability to achieve long-acting delivery.

$$\text{Equivalent Concentration}_{\text{SIM}} = \frac{\text{Equivalent SIM content} + \text{actual SIM content}}{V} \quad (9)$$

4.4. Estimation of actual patch size for humans

The estimation of two MNs for humans was predicted based on the results of *ex vivo* skin permeation and deposition studies of SIM. According to the FDA instructions (2012), the usual dose of simvastatin for adults is between 10 mg and 40 mg once a day. People with very high cholesterol levels may be prescribed a higher daily dose of 80 mg. The oral availability of SIM is approximately 5 %. To date, many double-blind, placebo-controlled and randomised crossover studies of SIM have employed a daily dose of 40 mg of SIM to patients (Backman et al., 2000). As a result, 40 mg/day was chosen as the oral dose for DMN and EMN patch size estimation. To provide an equivalent dose in humans, approximately 2 mg of SIM must be delivered from both types of MNs intradermally. Considering the permeation and deposition performance of DMNs in the *ex vivo* study, approximately 4.25 mg of SIM obtained from four DMNs with a total area of 3.04 cm². Accordingly, a patch of 20.02 cm² would be sufficient to provide therapeutically-relevant plasma concentrations of SIM over 2 weeks. Similarly, approximately 1.26 mg of SIM was provided by six EMNs with a total area of 1.5 cm². Therefore, the patch size of EMNs is estimated to be 33.3 cm² to achieve
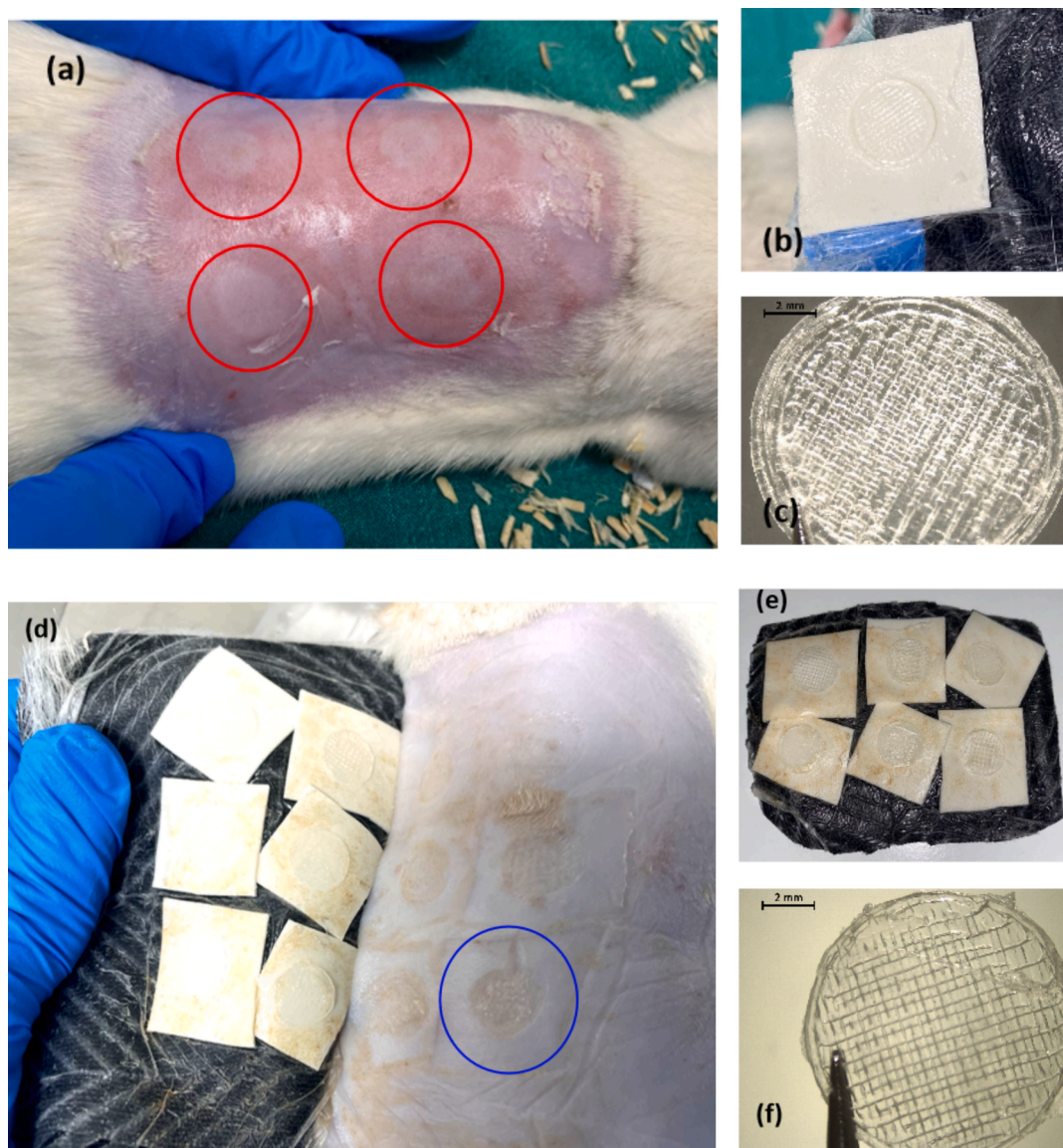
Fig. 11. Digital images and micrographs taken after applying 24 h of SIM NCs DMNs and SIM EMNs. (a) Application sites of SIM NCs DMNs on the dorsal skin of female *Sprague-Dawley* rats (white area within the red circles). (b) Digital images of the adhesive backing layer and baseplate after applying SIM NCs DMNs for 24 h. (c) Micrographs of the baseplate of SIM NCs DMNs. (d) Application sites of SIM EMNs (needle array traces within the blue circle). (e) Digital images of the adhesive backing layer and baseplate of SIM EMNs after 24 h of application. (f) Micrographs of the baseplate of SIM EMNs completely separated with needle tips.

Table 9

In vivo plasma pharmacokinetic parameters of SIMA after oral, SIM NCs loaded DMN, and SIM EMN administration to *Sprague–Dawley* female rats (means ± S. D., n = 6).

Parameters	Unit	Oral	DMNs	EMNs
C_{max}	ng/mL	1278.26 ± 471.25	228.72 ± 75.35	59.33 ± 6.32
T_{max}	h	1	2	4
AUC_{0-360}	ng/ml*h	5702.04 ± 1994.19	10667.26 ± 1316.20	5666.05 ± 1006.66

Table 10

In vivo plasma pharmacokinetic parameters of SIM after oral, SIM NCs loaded DMN, and SIM EMN administration to *Sprague–Dawley* female rats (means ± S. D., n = 6).

Parameters	Unit	Oral	DMNs	EMNs
C_{max}	ng/mL	220.66 ± 172.96	120.71 ± 76.97	150.25 ± 13.32
T_{max}	h	2	24	24
AUC_{0-360}	ng/ml*h	1312.50 ± 829.65	9062.51 ± 4210.58	12764.95 ± 7146.89

a therapeutic dose over 2 weeks. According to previous investigation from our group, large MN patches were successfully accepted and applied in human volunteers (Ripolin et al., 2017). As a result, both patch sizes are considered within the acceptable range and have the potential to achieve an efficient and sustained delivery to patients in a painless manner.

5. Conclusion

Low oral bioavailability has long been a major issue for SIM delivery, while low water solubility limits the diversity of development of its transdermal formulations. In this work, two MN strategies were applied to improve the bioavailability of SIM, simplify the fabrication process, and achieve long-term release. These studies involved NCs- loaded
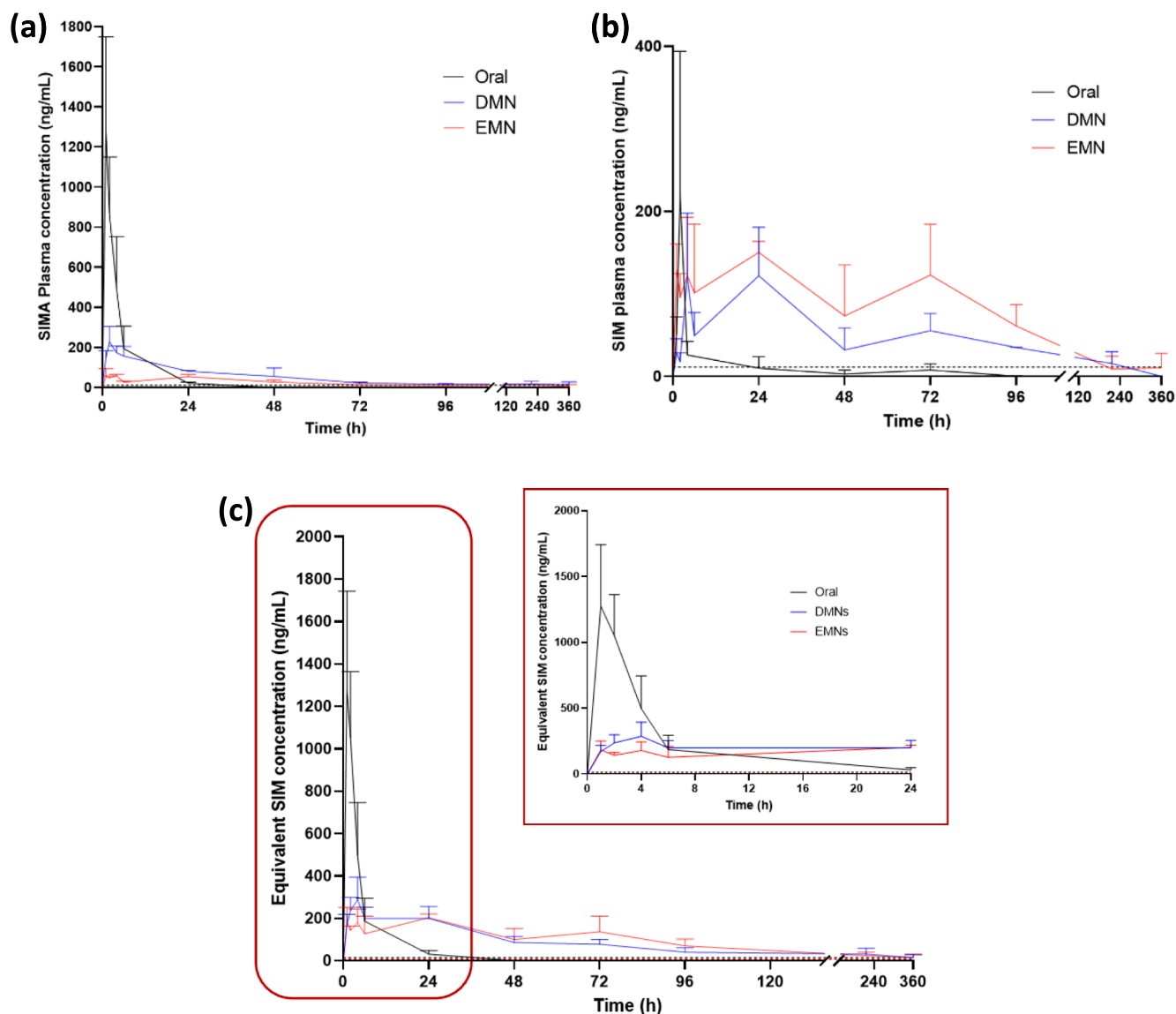
Fig. 12. The mean plasma concentration and time profiles of (a) SIMA and (b) SIM after oral administration of SIM suspension, four SIM NCs DMN applications, and six SIM EMN applications (means + S.D., n = 3 at 1, 2, 4 and 6 h, n = 6 at the remaining time points). The black dashed lines in the two figures represent the lower limits of quantification (LLOQ) for SIMA and SIM in the analytical method, which were 11.54 ng/ml and 14.24 ng/ml, respectively. (c) The mean plasma concentration and time profiles of equivalent SIM after oral administration of the SIM suspension, four DMN applications, and six EMN applications (means + S.D., n = 3 at 1, 2, 4 and 6 h, n = 6 at the remaining time points). The red dashed lines represent the maximum concentration of SIM in 10 healthy volunteers after a single oral dose of 40 mg of simvastatin (6.87 ng/ml) (Backman et al., 2000). The black dashed line is the LLOQ of SIM in the analytical method (14.24 ng/ml).

Table 11

In vivo plasma pharmacokinetic parameters of equivalent SIM integrated mathematically after the administration of oral cohort and two MN cohorts (means ± S.D., n = 6).

Parameter	Unit	Oral	DMN	EMN
Dose	mg/rat	16	10	2.58
T_{max}	Hour	1	4	24
C_{max}	ng/mL	1275.91 ± 466.78	287.39 ± 106.82	203.05 ± 17.07
AUC_{0-t}	ng/mL*h	6362.29 ± 1174.09	19309.82 ± 3276.83	21302.47 ± 3251.70

DMNs and, for the first time, the use of a novel EMN design. These included a comprehensive screening of SIM nanoformulations and successful development of a polymeric hollow shell for constituting EMNs. The addition of the effervescent agents significantly improved the permeability and in-skin deposition efficiency. For the *in vivo* studies, SIM was successfully delivered into female *Sprague–Dawley* rats *via* two MN strategies. Compared to oral delivery, MN cohorts can maintain therapeutically relevant concentrations over 15 days after a single-dose application for 24 h. Future studies could evaluate the treatment efficiency of MN-mediated delivery in a suitable model of hyperlipidaemia, and appropriate MN preparation techniques for mass production. These are the key factors in determining whether MN products can achieve commercial scale-up and be cost-effective.

CRediT authorship contribution statement

Nuoya Qin: Writing – review & editing, Writing – original draft, Methodology, Investigation, Formal analysis, Data curation, Conceptualization. **Mingshan Li:** Methodology, Investigation, Formal analysis, Data curation. **Lalitkumar K. Vora:** Writing – review & editing, Investigation, Formal analysis. **Ke Peng:** Methodology, Investigation. **Akmal Hidayat Bin Sabri:** Investigation, Formal analysis. **Yushi Tao:** Investigation. **Alejandro J. Paredes:** Writing – review & editing, Methodology, Investigation. **Helen O. McCarthy:** Resources. **Ryan F. Donnelly:** Writing – review & editing, Supervision, Resources, Methodology, Formal analysis, Conceptualization.

Declaration of competing interest

The authors declare that they have no known competing financial interests or personal relationships that could have appeared to influence the work reported in this paper.

Data availability

Data will be made available on request.

Acknowledgements

References

Abdelwahed, W., Degobert, G., Stainmesse, S., Fessi, H., 2006. Freeze-drying of nanoparticles: formulation, process and storage considerations. Adv. Drug Deliv. Rev. 58 (15), 1688–1713. https://doi.org/10.1016/j.addr.2006.09.017.

Afolabi, A., Akinlabi, O., Bilgili, E., 2014. Impact of process parameters on the breakage kinetics of poorly water-soluble drugs during wet stirred media milling: a microhydrodynamic view. Eur. J. Pharm. Sci. 51 (1), 75–86. https://doi.org/10.1016/j.ejps.2013.09.002.

Ahmad, A., Dhanalekshmi, U.M., Koumaravelu, K., Francis, A.P., Khan, S.A., Abuzinadah, M.F., Selvasudha, N., 2023. A study on pharmacokinetic functionalities and safety margins of an optimized simvastatin nanoformulation. Pharmaceuticals 16 (3), 380. https://doi.org/10.3390/ph16030380.

Backman, J.T., Kyrklund, C., Kivistö, K.T., Wang, J.S., Neuvonen, P.J., 2000. Plasma concentrations of active simvastatin acid are increased by gemfibrozil. Clin. Pharmacol. Ther. 68 (2), 122–129. https://doi.org/10.1067/mcp.2000.108507.

Belay, B., Belamarich, P.F., Tom-Revzon, C., 2007. The use of statins in pediatrics: knowledge base, limitations, and future directions. Pediatrics 119 (2), 370–380. https://doi.org/10.1542/peds.2006-0787.

Cárcamo-Martínez, Á., Mallon, B., Anjani, Q.K., Domínguez-Robles, J., Utomo, E., Vora, L.K., Tekko, I.A., Larrañeta, E., Donnelly, R.F., 2021. Enhancing intradermal delivery of tofacitinib citrate: comparison between powder-loaded hollow microneedle arrays and dissolving microneedle arrays. Int. J. Pharm. 593, 120152 https://doi.org/10.1016/j.ijpharm.2020.120152.

Chen, F., Yan, Q., Yu, Y., Wu, M.X., 2017. BCG vaccine powder-laden and dissolvable microneedle arrays for lesion-free vaccination. J. Control. Release 255, 36–44. https://doi.org/10.1016/j.jconrel.2017.03.397.

Eiland, L.S., Luttrell, P.K., 2010. Use of statins for dyslipidemia in the pediatric population. J. Pediatr. Pharmacol. Ther. 15 (3), 160–172. https://doi.org/10.5863/1551-6776-15.3.160.

Filppula, A.M., Hirvensalo, P., Parviainen, H., Ivaska, V.E., Lönnberg, K.I., Deng, F., Viinamäki, J., Kurkela, M., Neuvonen, M., Niemi, M., 2021. Comparative hepatic and intestinal metabolism and pharmacodynamics of statinsxs. Drug Metab. Dispos. 49 (8), 658–667. https://doi.org/10.1124/DMD.121.000406.

Hardy, J.G., Larrañeta, E., Donnelly, R.F., McGoldrick, N., Migalska, K., McCrudden, M. T.C., Irwin, N.J., Donnelly, L., McCoy, C.P., 2016. Hydrogel-forming microneedle arrays made from light-responsive materials for on-demand transdermal drug delivery. Mol. Pharm. 13 (3), 907–914. https://doi.org/10.1021/acs.molpharmaceut.5b00807.

He, Y., Chen, N., Zang, M., Zhang, J., Zhang, Y., Lu, H., Zhao, Q., Mao, Y., Yuan, Y., Wang, S., Gao, Y., 2024. Glucose-responsive insulin microneedle patches for long-acting delivery and release visualization. J. Control. Release 368. https://doi.org/10.1016/j.jconrel.2024.03.001.

Kaur, P., Garg, T., Rath, G., Murthy, R.S.R., Goyal, A.K., 2016. Development, optimization and evaluation of surfactant-based pulmonary nanolipid carrier system of paclitaxel for the management of drug resistance lung cancer using Box-Behnken design. Drug Deliv. 23 (6), 1912–1925. https://doi.org/10.3109/10717544.2014.993486.

Kim, S., Eum, J., Yang, H., Jung, H., 2019. Transdermal finasteride delivery via powder-carrying microneedles with a diffusion enhancer to treat androgenetic alopecia. J. Control. Release 316, 118–125. https://doi.org/10.1016/j.jconrel.2019.11.002.

Kim, S., Yang, H., Eum, J., Ma, Y., Fakhraei Lahiji, S., Jung, H., 2020. Implantable powder-carrying microneedles for transdermal delivery of high-dose insulin with enhanced activity. Biomaterials 232, 119733. https://doi.org/10.1016/J.BIOMATERIALS.2019.119733.

Kolarsick, P.A.J., Kolarsick, M.A., Goodwin, C., 2011. Anatomy and physiology of the skin. J. Dermatol. Nurses. Assoc. 3 (4), 203–213.

Larrañeta, E., Moore, J., Vicente-Pérez, E.M., González-Vázquez, P., Lutton, R., Woolfson, A.D., Donnelly, R.F., 2014. A proposed model membrane and test method for microneedle insertion studies. Int. J. Pharm. 472 (1–2), 65–73. https://doi.org/10.1016/j.ijpharm.2014.05.042.

Larrañeta, E., Lutton, R.E.M., Woolfson, A.D., Donnelly, R.F., 2016. Microneedle arrays as transdermal and intradermal drug delivery systems: materials science, manufacture and commercial development. Mater. Sci. Eng. R Reports 104, 1–32. https://doi.org/10.1016/j.mser.2016.03.001.

Li, W., Tang, J., Terry, R.N., Li, S., Brunie, A., Callahan, R.L., Noel, R.K., Rodríguez, C.A., Schwendeman, S.P., Prausnitz, M.R., 2019. Long-acting reversible contraception by effervescent microneedle patch. Sci. Adv. 5(11), eaaw8145. doi: 10.1126/sciadv.aaw8145.

Li, M., Vora, L.K., Peng, K., Donnelly, R.F., 2022. Trilayer microneedle array assisted transdermal and intradermal delivery of dexamethasone. Int. J. Pharm. 612, 121295 https://doi.org/10.1016/j.ijpharm.2021.121295.

Li, J., Wang, Z., Zhang, H., Gao, J., Zheng, A., 2021. Progress in the development of stabilization strategies for nanocrystal preparations. Drug Deliv. 28 (1), 19–36. https://doi.org/10.1080/10717544.2020.1856224.

Liu, M., Su, X., Li, G., Zhao, G., Zhao, L., 2015. Validated UPLC-MS/MS method for simultaneous determination of simvastatin, simvastatin hydroxy acid and berberine in rat plasma: application to the drug-drug pharmacokinetic interaction study of simvastatin combined with berberine after oral administratio. J. Chromatogr. B Anal. Technol. Biomed. Life Sci. 1006, 8–15. https://doi.org/10.1016/j.jchromb.2015.09.033.

Malamatari, M., Taylor, K.M.G., Malamataris, S., Douroumis, D., Kachrimanis, K., 2018. Pharmaceutical nanocrystals: production by wet milling and applications. Drug Discov. Today 23 (3), 534–547. https://doi.org/10.1016/j.drudis.2018.01.016.

McGuckin, M.B., Wang, J., Ghanma, R., Qin, N., Palma, S.D., Donnelly, R.F., Paredes, A. J., 2022. Nanocrystals as a master key to deliver hydrophobic drugs via multiple administration routes. J. Control. Release 345, 334–353. https://doi.org/10.1016/j.jconrel.2022.03.012.

Moon, S.J., Lee, S.H., Jang, K., Yu, K.S., Yim, S.V., Kim, B.H., 2017. Comparative pharmacokinetic and tolerability evaluation of two simvastatin 20 mg formulations in healthy Korean male volunteers. Transl. Clin. Pharmacol. 25 (1), 10. https://doi.org/10.12793/tcp.2017.25.1.10.

Müller, R.H., Gohla, S., Keck, C.M., 2011. State of the art of nanocrystals – special features, production, nanotoxicology aspects and intracellular delivery. Eur. J. Pharm. Biopharm. 78 (1), 1–9. https://doi.org/10.1016/j.ejpb.2011.01.007.

Owens, A.P., Byrnes, J.R., Mackman, N., 2014. Hyperlipidemia, tissue factor, coagulation, and simvastatin. Trends Cardiovasc. Med. 24 (3), 95–98. https://doi.org/10.1016/j.tcm.2013.07.003.

Pailler-Mattei, C., Bec, S., Zahouani, H., 2008. In vivo measurements of the elastic mechanical properties of human skin by indentation tests. Med. Eng. Phys. 30 (5), 599–606. https://doi.org/10.1016/j.medengphy.2007.06.011.

Paredes, A.J., McKenna, P.E., Ramöller, I.K., Naser, Y.A., Volpe-Zanutto, F., Li, M., Abbate, M.T.A., Zhao, L., Zhang, C., Abu-Ershaid, J.M., Dai, X., Donnelly, R.F., 2021. Microarray patches: poking a hole in the challenges faced when delivering poorly soluble drugs. Adv. Funct. Mater. 31 (1), 2005792. https://doi.org/10.1002/adfm.202005792.

Parker, B.A., Capizzi, J.A., Grimaldi, A.S., Clarkson, P.M., Cole, S.M., Keadle, J., Chipkin, S., Pescatello, L.S., Simpson, K., Michael White, C., Thompson, P.D., 2013. Effect of statins on skeletal muscle function. Circulation 127 (1), 96–103. https://doi.org/10.1161/CIRCULATIONAHA.112.136101.

Pereira, M.N., Schulte, H.L., Duarte, N., Lima, E.M., Sá-Barreto, L.L., Gratieri, T., Gelfuso, G.M., Cunha-Filho, M.S.S., 2017. Solid effervescent formulations as new approach for topical minoxidil delivery. Eur. J. Pharm. Sci. 96, 411–419. https://doi.org/10.1016/j.ejps.2016.10.016.

Plakkot, S., De Matas, M., York, P., Saunders, M., Sulaiman, B., 2011. Comminution of ibuprofen to produce nano-particles for rapid dissolution. Int. J. Pharm. 415 (1–2), 307–314. https://doi.org/10.1016/j.ijpharm.2011.06.002.

Ramöller, I.K., Volpe-Zanutto, F., Vora, L.K., Abbate, M.T.A., Hutton, A.R.J., McKenna, P. E., Peng, K., Tekko, I.A., Sabri, A., McAlister, E., McCarthy, H.O., Paredes, A.J., Donnelly, R.F., 2024. Intradermal delivery of the antiretroviral drugs cabotegravir and rilpivirine by dissolving microarray patches: investigation of lymphatic uptake. J. Control. Release 366. https://doi.org/10.1016/j.jconrel.2024.01.010.

Ripolin, A., Quinn, J., Larrañeta, E., Vicente-Perez, E.M., Barry, J., Donnelly, R.F., 2017. Successful application of large microneedle patches by human volunteers. Int. J. Pharm. 521 (1–2), 92–101. https://doi.org/10.1016/j.ijpharm.2017.02.011.

Shattat, G.F., 2014. A review article on hyperlipidemia: Types, treatments and new drug targets. Biomed. Pharmacol. J. 7 (2), 399–409. https://doi.org/10.13005/bpj/504.

Shitara, Y., Sugiyama, Y., 2006. Pharmacokinetic and pharmacodynamic alterations of 3-hydroxy-3-methylglutaryl coenzyme A (HMG-CoA) reductase inhibitors: drug-drug interactions and interindividual differences in transporter and metabolic enzyme functions. Pharmacol. Ther. 112 (1), 71–105. https://doi.org/10.1016/j.pharmthera.2006.03.003.

Simões, R.G., Bernardes, C.E.S., Joseph, A., Piedade, M.F.M., Kraus, W., Emmerling, F., Diogo, H.P., Da Piedade, M.E.M., 2018. Polymorphism in simvastatin: twinning,

disorder, and enantiotropic phase transitions. Mol. Pharm. 15 (11) https://doi.org/10.1021/acs.molpharmaceut.8b00818.

Sinzinger, H., Wolfram, R., Peskar, B.A., 2002. Muscular side effects of statins. J. Cardiovasc. Pharmacol. 40 (2), 163–171. https://doi.org/10.1097/00005344-200208000-00001.

Trenkenschuh, E., Friess, W., 2021. Freeze-drying of nanoparticles: how to overcome colloidal instability by formulation and process optimization. Eur. J. Pharm. Biopharm. 165, 345–360. https://doi.org/10.1016/j.ejpb.2021.05.024.

Vora, L.K., Donnelly, R.F., Larrañeta, E., González-Vázquez, P., Thakur, R.R.S., Vavia, P. R., 2017. Novel bilayer dissolving microneedle arrays with concentrated PLGA nano-microparticles for targeted intradermal delivery: proof of concept. J. Control. Release 265, 93–101. https://doi.org/10.1016/j.jconrel.2017.10.005.

Vora, L.K., Vavia, P.R., Larrañeta, E., Bell, S.E.J., Donnelly, R.F., 2018. Novel nanosuspension-based dissolving microneedle arrays for transdermal delivery of a hydrophobic drug. J. Interdiscip. Nanomedicine 3 (2), 89–101. https://doi.org/10.1002/jin2.41.

Wang, Q., Ellis, P.R., Ross-Murphy, S.B., 2003. Dissolution kinetics of guar gum powders - II. Effects of concentration and molecular weight. Carbohydr. Polym. 53 (1), 75–83. https://doi.org/10.1016/S0144-8617(03)00009-2.

Wang, Q.L., Zhu, D.D., Liu, X.B., Chen, B.Z., Guo, X.D., 2016. Microneedles with controlled bubble sizes and drug distributions for efficient transdermal drug delivery. Sci. Rep. 6 (1), 38755. https://doi.org/10.1038/srep38755.

Ward, N.C., Watts, G.F., Eckel, R.H., 2019. Statin toxicity: mechanistic insights and clinical implications. Circ. Res. 124 (2), 328–350. https://doi.org/10.1161/CIRCRESAHA.118.312782.

Yebyo, H.G., Aschmann, H.E., Kaufmann, M., Puhan, M.A., 2019. Comparative effectiveness and safety of statins as a class and of specific statins for primary prevention of cardiovascular disease: a systematic review, meta-analysis, and network meta-analysis of randomized trials with 94,283 participants. Am. Heart J. 210, 18–28. https://doi.org/10.1016/j.ahj.2018.12.007.

Yu, Y.Q., Yang, X., Wu, X.F., Fan, Y.B., 2021. Enhancing permeation of drug molecules across the skin via delivery in nanocarriers: novel strategies for effective transdermal applications. Front. Bioeng. Biotechnol. 9, 646554 https://doi.org/10.3389/fbioe.2021.646554.

Zhang, Y., Huo, M., Zhou, J., Xie, S., 2010. PKSolver: An add-in program for pharmacokinetic and pharmacodynamic data analysis in Microsoft Excel. Comput. Methods Programs Biomed. 99 (3), 306–314. https://doi.org/10.1016/j.cmpb.2010.01.007.

Zhang, C., Jahan, S.A., Zhang, J., Bianchi, M.B., Volpe-Zanutto, F., Baviskar, S.M., Rodriguez-Abetxuko, A., Mishra, D., Magee, E., Gilmore, B.F., Singh, T.R.R., Donnelly, R.F., Larrañeta, E., Paredes, A.J., 2023a. Curcumin nanocrystals-in-nanofibres as a promising platform for the management of periodontal disease. Int. J. Pharm. 648, 123585 https://doi.org/10.1016/j.ijpharm.2023.123585.

Zhang, C., Vora, L.K., Tekko, I.A., Volpe-Zanutto, F., Peng, K., Paredes, A.J., McCarthy, H.O., Donnelly, R.F., 2023b. Development of dissolving microneedles for intradermal delivery of the long-acting antiretroviral drug bictegravir. Int. J. Pharm. 642, 123108 https://doi.org/10.1016/j.ijpharm.2023.123108.

Zhang, Y., Wang, H., Gao, C., Li, X., Li, L., 2013. Highly ordered mesoporous carbon nanomatrix as a new approach to improve the oral absorption of the water-insoluble drug, simvastatin. Eur. J. Pharm. Sci. 49 (5), 864–872. https://doi.org/10.1016/j.ejps.2013.05.031.